Ore Geology Reviews 77 (2016) 332–349

Contents lists available at ScienceDirect

Ore Geology Reviews

journal homepage: www.elsevier.com/locate/oregeorev

Structural controls of fluid flow and gold mineralization in the easternmost parts of the Karagwe-Ankole Belt of north-western Tanzania

Corné Koegelenberg [a,*], Alexander F.M. Kisters [a], Chris Harris [b]

[a] Department of Earth Science, Stellenbosch University, Private Bag X1, Matieland 7620, South Africa
[b] Department of Geological Sciences, University of Cape Town, Private Bag X3, Rondebosch 7701, South Africa

ARTICLE INFO

Article history:
Received 7 December 2015
Received in revised form 6 March 2016
Accepted 11 March 2016
Available online 17 March 2016

ABSTRACT

Gold mineralization in the Biharamulo region of western Tanzania is confined to the sheared, low-angle basement-cover contact between Archaean basement gneisses of the Tanzania Craton and the structurally overlying, low-grade metamorphic metasediments of the Mesoproterozoic Karagwe-Ankole Belt. Regional-scale fluid flow along this detachment is indicated by the pervasive silicification and retrogression of wall rocks to pervasively foliated phyllonites and pyritization of particularly metasediments, commonly graphite-rich, in the hanging wall of the shear zone. Gold mining centres on specific structural sites along the detachment, but also in stratigraphically higher sections in the structurally overlying metasediments. Zones of gold mineralization along the detachment correlate with NE trending ramp structures (dip angles 20°–35°) that are most ideally orientated for slip and reactivation within the low-angle phyllonitic detachment. Repeatedly overprinted auriferous quartz-vein stockworks in quartzofeldspathic gneisses immediately below the detachment indicate brittle fracturing of the competent footwall lithotypes during slip along the weaker detachment. In cases of massive silicification, up to 50 m thick quartz blows are formed along the contacts between detachment phyllonites and footwall gneisses. The multiple overprinting relationships of successive quartz-vein generations in these zones of massive silicification suggests that the quartz blows acted as competent blocks in the weak detachment, causing the repeated overprint of earlier silicification by later fracturing and quartz-veining events. Gold mineralization above the detachment and in stratigraphically higher metasediments is closely associated with fold structures that form part of the low-grade metamorphic fold-and-thrust belt. Veining is particularly abundant in competent lithotypes, such as quartzite and chemically reactive ferruginous mafic sills. Overprinting relationships between quartz vein sets illustrate fluid flow during fold amplification and, importantly, the final lock-up stage of folds, during which much of the mineralization was introduced. Oxygen isotope values for quartz veins indicate fluids were likely derived from clastic, mainly metapelitic sedimentary sequences of the Karagwe-Ankole Fold Belt. The data also implies that the partially reworked Archaean granitoid-greenstone basement of the Tanzania Craton has not contributed to the fluid evolution and possibly gold mineralization. The extent (>100 km) of the basement-cover detachment and associated alteration is indicative for a regional-scale fluid system. Gold mineralization is, however, controlled by local structures and lithological contrasts that require the detailed mapping and sampling of the regional structure.

1. Introduction

Tanzania is Africa's 4th largest gold producer with an annual production of ca. 40 tonne Au (Tanzania Chamber of Minerals and Energy, 2015). Some 90% of the gold production comes from late-Archaean greenstone belts of the Tanzania Craton (TC), mainly from the Lake Victoria region and the Lake Nyanza- and East Lake Victoria Superterranes (Borg and Shackleton, 1997; Borg and Krogh, 1999; Kabete et al., 2012). There have been very few recent gold discoveries on the TC and the apparent maturation of gold exploration on the craton has shifted exploration efforts towards the less explored margins of the TC (Kabete et al., 2012) (Fig. 1). For the most part, the TC is bordered by younger orogenic belts including the Pan-African Mozambique Belt in the east (Fritz et al., 2013) and the Paleoproterozoic Usagaran-, Ubendian-, Rusizian- and Ruwenzori Belts from the southern to north-western margins of the TC (e.g., De Waele et al., 2008, and references therein) (Fig. 1). These are mostly deeply eroded amphibolite- and granulite-facies terrains with somewhat limited potential for hydrothermal gold mineralization compared to the greenschist-facies deposits of the TC. In contrast, low-grade metamorphic, late Paleo- to Mesoproterozoic fold-and-thrust belts and foreland basins unconformably or structurally overlie much of the western parts of the TC. These

* Corresponding author.
E-mail addresses: cornekoegelenberg@tect.co.za (C. Koegelenberg), akisters@sun.ac.za (A.F.M. Kisters), chris.harris@uct.ac.za (C. Harris).

http://dx.doi.org/10.1016/j.oregeorev.2016.03.010
0169-1368/

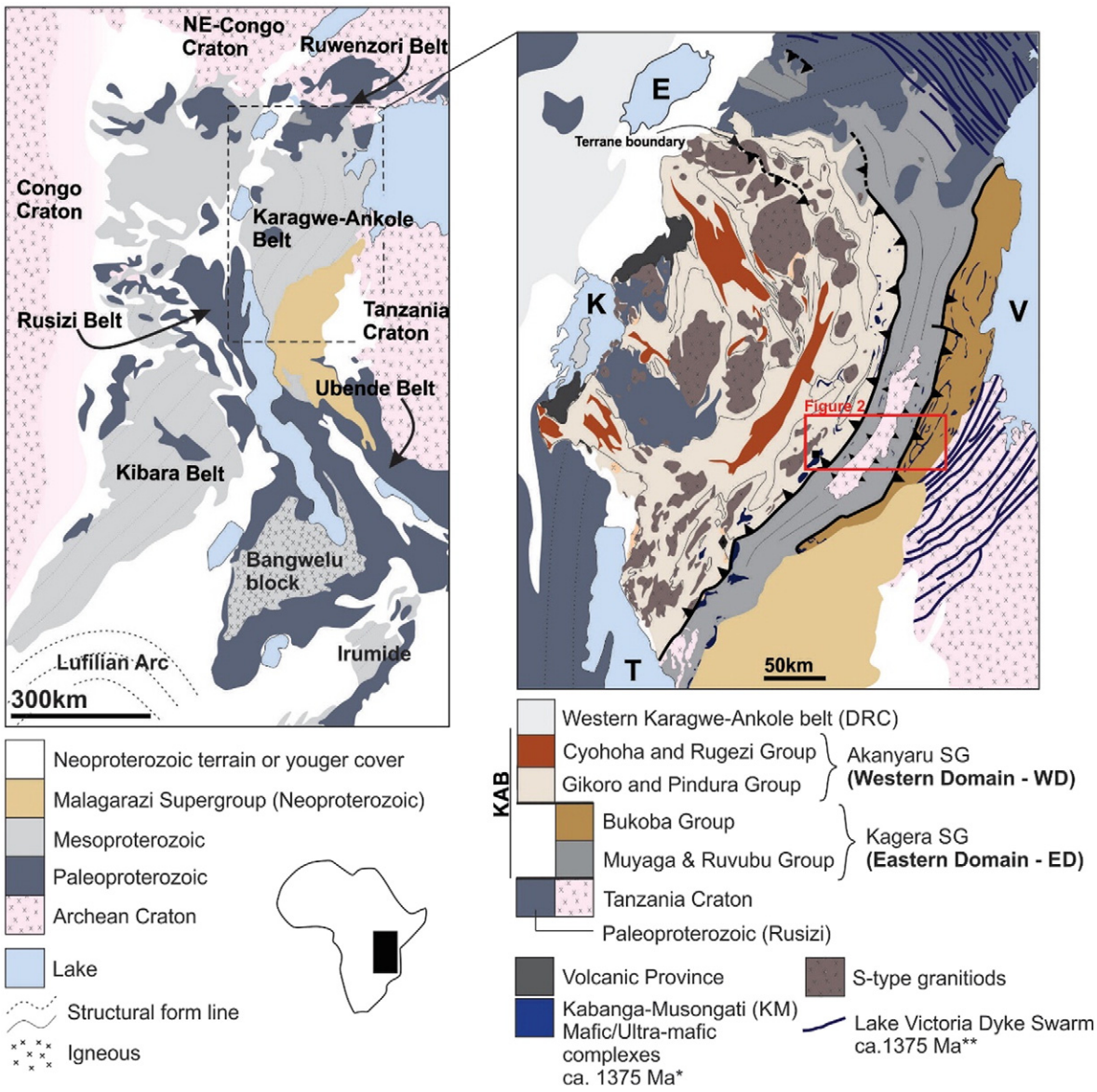

Fig. 1. Regional geological framework of central-east Africa and the Karagwe-Ankole Belt (KAB). Geological maps modified after *Tack et al. (2010); Fernandez-Alonso et al. (2012) and **Mäkitie et al. (2014). Lakes: Kivu (K); Tanganyika (T); Edward (E); Victoria (V).

belts belong to the broader Mesoproterozoic Kibara system (sensu lato) (Cahen et al., 1984; Tack et al., 2010; Fernandez-Alonso et al., 2012).

The Karagwe-Ankole Belt (KAB) (sensu stricto) represents the northernmost segment of the Kibara system (Tack et al., 1994) (Fig. 1). The eastern margin of the KAB overlies basement gneisses of the TC along a broadly flatlying, mylonitic detachment. This detachment is well exposed in and around the regional-scale structural window of the Mugera-Nyakahura (MN) inlier where Archaean basement outcrops over a strike length of >100 km below the low-grade rocks of the eastern KAB (Fig. 2; Kabete et al., 2012; Koegelenberg and Kisters, 2014). Pervasive silicification and alteration of both basement gneisses and commonly graphitic metasedimentary rocks of the KAB around much of the MN inlier testify to regional-scale fluid flow (e.g. Koegelenberg and Kisters, 2014). Artisanal gold mining operations target both the highly silicified detachment zone and the overlying rocks of the KAB and can be traced for several tens of kilometres along strike of the basement cover contact. However, mining is highly focused on smaller sections of the basement-cover contact suggesting distinct controls and focusing of the regional-scale fluid flow and associated gold mineralization around the MN inlier.

The aim of this paper is to characterize the structural controls of fluid flow along the basement cover contact around the MN inlier in the Biharamulo region in NW Tanzania as a potentially regionally significant gold mining district. Detailed case histories around existing mining camps are used to highlight the structural controls of fluid flow and mineralization in specific sites of known gold mineralization. Whole-rock and mineral oxygen isotope data are used to constrain possible fluid sources for the mineralization.

2. Regional geology of the Karagwe-Ankole Belt's eastern domain

The Archaean granitoid-greenstone basement of the western TC is structurally and/or unconformably overlain by the eastern extremities of the Mesoproterozoic Karagwe-Ankole fold-and-thrust belt. In the Biharamulo region, basement rocks are exposed in the regional- scale (ca. 100 × 20 km) Mugera-Nyakahura inlier (Fig. 2). Rocks of the easternmost Karagwe-Ankole Fold Belt comprise a low-grade metamorphic, multiply deformed, up to 2.5 km thick Paleo- to Mesoproterozoic sequence of pelites, psammites and minor volcanic rocks assigned to the Kagera Supergroup (Tack et al., 2010; Fernandez-Alonso et al.,

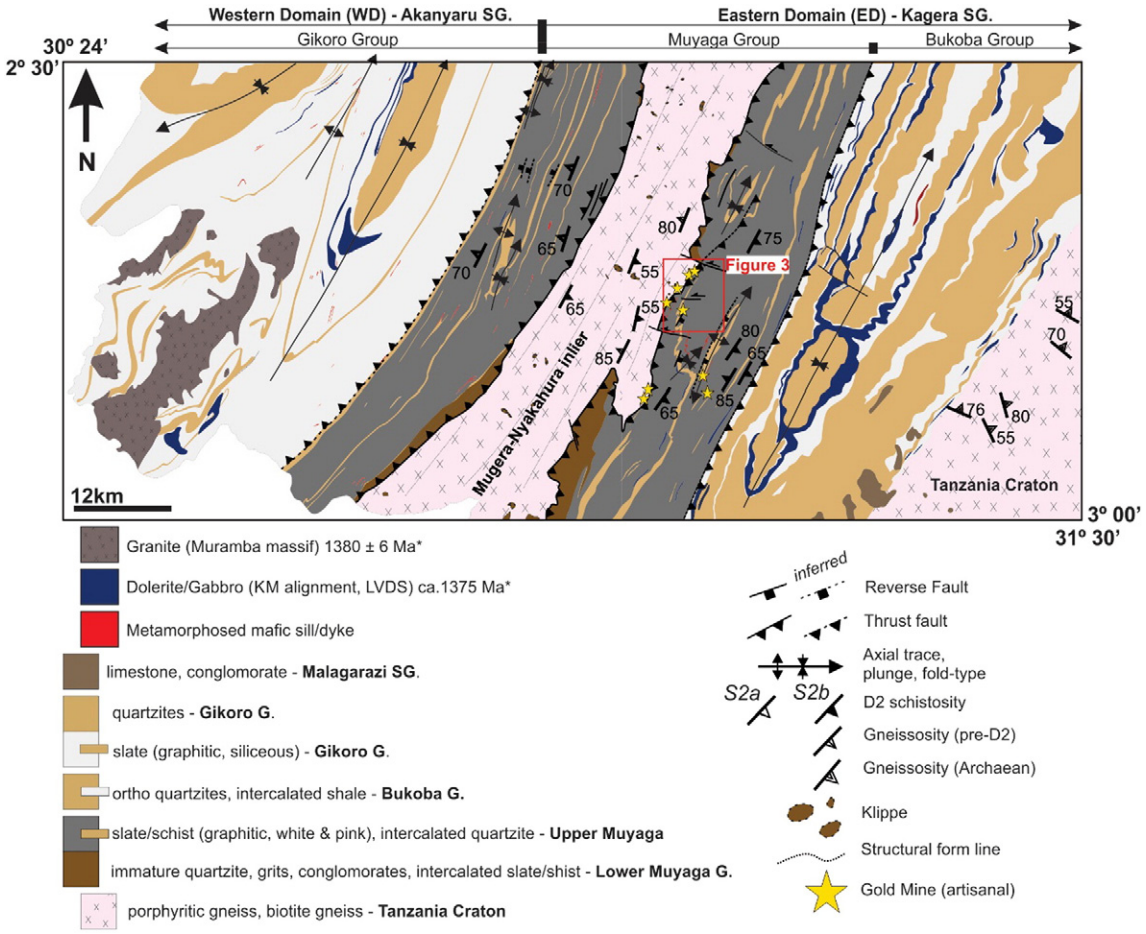

Fig. 2. Geology of the Western- and Eastern Domain (WD and ED) of the Karagwe-Ankole Belt, NW Tanzania, with locations of artisanal gold mines. Modified after Koegelenberg and Kisters (2014). Ages after *Tack et al. (2010) and geological groupings of the WD after Fernandez-Alonso et al. (2012).

2012; Koegelenberg et al., 2015). The meta-sediments have been intruded by ca. 1375–1380 Ma mafic sills and dykes of the Lake Victoria Dyke Swarm (Deblond et al., 2001; Tack et al., 2010; Mäkitie et al., 2014). In the eastern KAB, the mafic rocks have been deformed and metamorphosed during the subsequent main phase of tectonism (D2) at ca. 1350 Ma (Evans et al., 2000; Koegelenberg et al., 2015). Co-eval granite plutonism between 1350 and 1380 Ma is only recorded from the high-grade metamorphic (amphibolite-facies) Akanyaru Supergroup of the Western Domains of the KAB, but is absent for the low-grade Kagera Supergroup in the east.

The decrease in metamorphic grade coincides with the decrease in deformation and fabric intensity of D2 structures from west to east and from the Akanyaru- into the Kagera Supergroup corresponding to the frontal termination of the KAB to the east and over the TC (Tack et al., 1994; Koegelenberg and Kisters, 2014). D2 structures and fabrics in the KAB record top-to-the-east thrusting and associated folding and fabric development related to the east-vergent propagation of the KAB over the western margin of the TC. The eastern termination of the KAB is developed as a km-scale triangle zone in which the Archaean MN basement inlier forms a tectonic wedge bounded by foreland (SE)-verging thrusts in the floor and hinterland (NW)-verging backthrusts at the top and in the roof (Koegelenberg and Kisters, 2014). The timing of the D2 tectonic event is controversial (e.g. Fernandez-Alonso et al., 2012), but Ar-Ar age data from the main detachment zone suggest the main phase of fold-and-thrust belt formation at ca. 1326 Ma (Koegelenberg et al., 2015). Younger thermal events and associated granite plutonism at ca. 1000 Ma seem restricted to the Western Domain (Tack et al., 2010) but are not recorded in the ED of the KAB (Koegelenberg et al., 2015).

3. Geology of the Biharamulo District, NW Tanzania

3.1. Tectonostratigraphy

3.1.1. Mugera-Nyakahura inlier

The geology of the western Biharamulo District can be sub-divided into three main, structurally overlying tectonostratigraphic units, namely (1) Archaean basement gneisses of the MN inlier, interpreted to form part of the western TC, overlain by (2) tightly folded and thrusted, low-grade metamorphic rocks of the Muyaga Group that are, in the east, underthrusted below (3) only very gently folded, mainly coarse-clastic succession of the Bukoba Group. The latter two constitute the Paleoproterozoic Kagera Supergroup of the eastern KAB (Fig. 2) (Fernandez-Alonso et al., 2012; Koegelenberg and Kisters, 2014; Koegelenberg et al., 2015). Gold mineralization is confined to the basement-cover contact and the lower parts of the Muyaga Group.

Archaean gneisses of the MN inlier were previously interpreted as an erosional window through the structurally overlying KAB (e.g. Figs. 3 and 5). More recently, Koegelenberg and Kisters (2014) recognized the regional change of fold-and-thrust vergence centred around the MN inlier and interpreted the basement gneisses as the roof of an eastward transported and ramped-up basement wedge (Fig. 2). Rocks of the MN inlier are commonly deeply weathered. River sections and isolated pavements expose fine crystalline, leucocratic biotite gneisses and

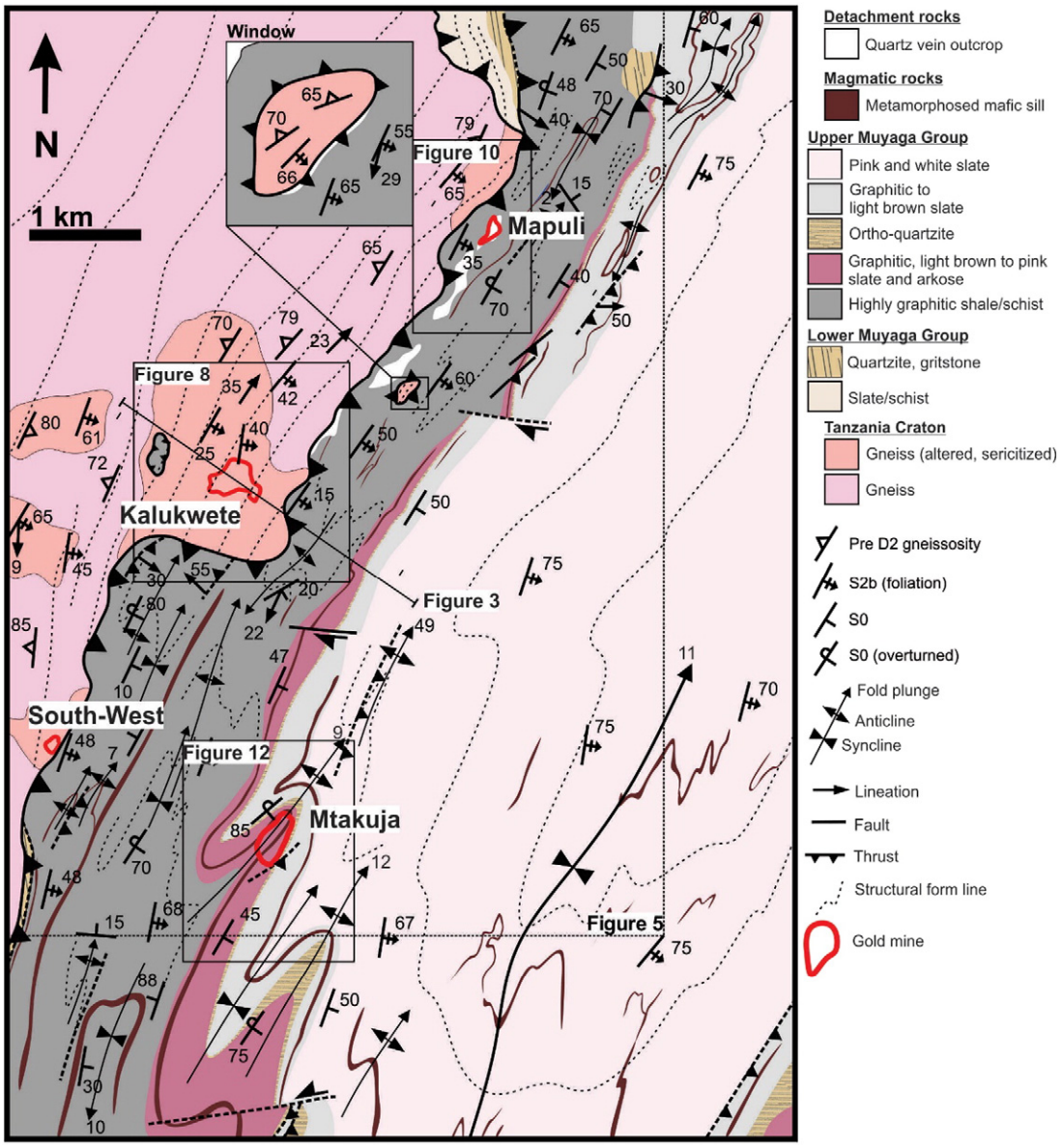

Fig. 3. Geology of the eastern margin of the Mugera-Nyakahura inlier and basement-cover detachment with Mapuli-, Kalukwete- and Mtakuja artisanal mines. Note South-West artisanal mine is not discussed due to the limited extent of the workings.

coarser, commonly cataclastic augen gneisses of trondhjemitic to granodioritic composition (Fig. 3) (Kabete et al., 2012). Primary mineral assemblages are quartz, plagioclase, biotite, hornblende and, in case of more granodioritic compositions, K-feldspar. Highly weathered amphibole and/or chlorite schists and amphibolites in the northern parts of the MN inlier have tentatively been correlated with greenstone lithotypes, similar to those of the Lake Nyanza Super Terrane of the TC to the immediate east of the KAB (Kabete et al., 2012).

3.1.2. Muyaga Group

The ca. 1780 Ma old Muyaga Group forms the lowermost sequence of the Kagera Supergroup (Fernandez-Alonso et al., 2012) and can be subdivided into a lithologically distinct Lower- and Upper Muyaga Group (Figs. 3 and 4) (Koegelenberg and Kisters, 2014). The Lower Muyaga Group (also the Kiganga Formation, after Westerhof et al., 2014, in Uganda) is a mainly coarse-clastic sequence made up of conglomerates, grits and impure quartzites interlayered with grey slate units. Cross-ripple lamina and asymmetrical ripples are common in quartzites and indicative of a fluvial to shallow marine setting. Intense folding and imbrication complicates thickness estimates for the Muyaga Group, but a minimum thickness of ca. 100 m seems likely. Unconformable contacts between the mainly coarse-clastic cover rocks and basement gneisses are reported from the southern parts of the MN inlier (Fernandez-Alonso et al., 2012), but much of the Lower Muyaga Group is absent further north, probably due to tectonic excision (Koegelenberg and Kisters, 2014).

The Lower Muyaga Group fines upwards into the ca. 2 km thick slate dominated Upper Muyaga Group (correlating with the Rakai Formation of Westerhof et al., 2014, in Uganda). The base of the Upper Muyaga Group is defined by a distinct, up to 300 m thick sequence of dark and highly graphitic slate units. Higher up in the succession, the slates are intercalated with isolated, but up to 15 m thick arkoses and/or mature quartzites that form distinct marker horizons (Koegelenberg and Kisters, 2014). The upper parts of the Upper Muyaga Group are

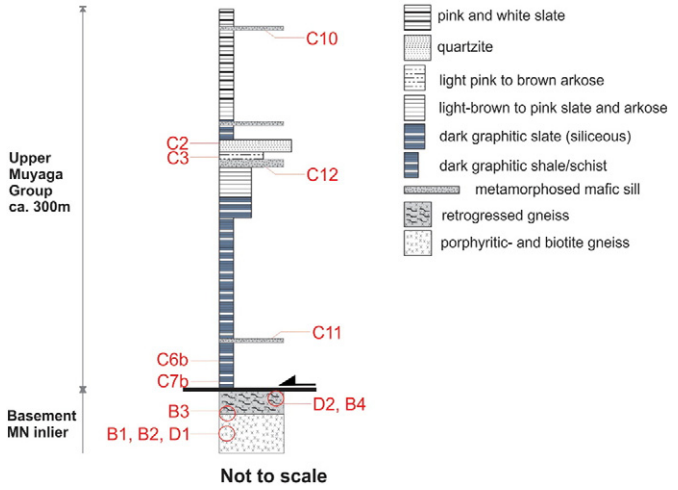

Fig. 4. Litho-stratigraphical log of the foot- and hanging wall of the detachment with sample locations of quartz veins and wall rock for oxygen isotope analysis (section location on Fig. 3).

dominated by a ca. 1.5 km thick, finely laminated and well bedded succession of pink to white-grey slate with subordinate arkose and ortho-quartzite units.

Towards the east, the Muyaga Group forms an underthrusted wedge structurally overlain by the ca. 2 km thick mainly coarse-clastic, thickly bedded and only gently folded Bukoba Group (Koegelenberg and Kisters, 2014).

3.2. Structure

Archaean basement gneisses and the overlying Muyaga Group are separated by a 20–50 m wide, gently undulating (see below) D2 detachment zone. Reworked Archaean basement gneisses below the detachment record at least 2 distinct periods of seemingly co-axial deformation (e.g. Pre-D2 vs. D2). The oldest episode is indicated by a steep west dipping to upright (pre-D2) gneissosity trending broadly NNE to NE across the MN inlier. Associated shearing is accommodated by mylonite bands and cataclasites in the coarse augen gneisses, showing top-to-the-SE kinematics. Notably these NE gneissic trends are at high angles to structural grain of the TC and may be the result of the thick-skinned thrusting and subsequent reworking of the northwestern margin of the TC during the 2.2–1.8 Ga Eburnean Orogeny (Koegelenberg et al., 2015).

The overlying Muyaga Group is part of the regional scale, D2a, SE-verging, fold-and-thrust belt of the KAB. However, folding along the eastern MN inlier margin forms part of a, D2b, regional and top-to-the-NW verging back-thrusted domain (Koegelenberg and Kisters, 2014). Associated F2b folds are tight and near recumbent along the base, but stratigraphically higher and to the east, folding progressively becomes more open with a steepening of the axial planar S2b foliation. Notably, tight, overturned and strongly north-west verging F2b folds are still recorded laterally within ca. 3 km east of the roof detachment and into the Upper Muyaga Group. Pervasive NW verging axial planar foliations (S2b), sub-horizontal and N to NNE trending intersection lineations ($L2b_i$) are well developed and correspond with top-to-the-NW tectonic transport and D2 backthrusting of the cover rocks on top of the basement gneisses (Koegelenberg and Kisters, 2014) (see below).

The detachment that marks the basement-cover contact is defined by an up to 50 m thick unit of imbricated muscovite-chlorite schists, phyllonites and mylonites (Koegelenberg and Kisters, 2014) (Fig. 3). Deformation and associated fluid flow has also caused near-pervasive retrogression of quartzo-feldspathic footwall gneisses to muscovite-(sericite) and/or muscovite-chlorite schists to a depth up to 30 m below the actual detachment. The detachment is characterized by a pervasive shallow SE dipping schistosity (S2b) and a shallow, mainly SE plunging stretching lineation (L2b) developed on the foliation plane. Shear sense indicators include mainly S-C′ fabrics and rotated quartz clasts in mylonites and/or phyllonites and record top-to-the-NW kinematics corresponding to north-westwards backthrusting of the Muyaga Group on top of the basement wedge.

3.3. Metamorphism

Phyllonites and mylonites in the detachment are characterized by quartz-sericite-chlorite-albite assemblages (Fig. 6a, b), mainly derived from the retrogression of original plagioclase-K-feldspar-biotite and/or hornblende-bearing assemblages of the underlying gneisses (Koegelenberg et al., 2015). The absence of biotite in phyllonites derived from gneisses suggests T conditions of ca. <400 °C during deformation and retrogression (Powell and Evans, 1983; Coggon and Holland, 2002). This corresponds to deformation textures in the basal detachment. Quartz is dynamically recrystallized and forms, in places, quartz ribbons that define the high-strain foliation (S2b). Quartzofeldspathic gneisses in the immediate footwall of the detachment, in turn, show pervasive cataclastic textures. Metapelites of the Muyaga Group are phyllitic, in places, showing similar quartz-sericite-chlorite-albite assemblages. Original igneous assemblages in metamafic sills and dykes in the Muyaga Group are replaced by tremolite-actinolite-chlorite-epidote-carbonate assemblages and plagioclase is pervasively saussuritised. These assemblages are not very well suited to tightly constrain P-T conditions, but both mineral parageneses and deformation textures point to lower-greenschist-facies metamorphic conditions during the overall D2 fold-and-thrust event.

4. Artisanal mining

4.1. Description of mines

Artisinal mining operations target auriferous quartz veins at two structural levels in (1) the sheared basement-cover contact; and (2) stratigraphically higher sections in rocks of the overlying Muyaga Group (Fig. 3).

The Kalukwete and Mapuli prospects illustrate different styles and controls of Au mineralization in the detachment along the basement-cover contact (Fig. 3). Kalukwete is the largest mining camp in the region located in basement gneisses in the immediate footwall of the main detachment. The gneisses are exposed in an erosional window through dark graphitic schists at the base of the Upper Muyaga Group. The Mapuli mine is located some 3 km north of Kalukwete, but is hosted in graphitic schists that form the base of the Upper Muyaga Group in the immediate hanging wall of the detachment. Mining operations of the Mtakuja prospect are located stratigraphically higher and away from the detachment in rocks of the Upper Muyaga Group, some 2 km east of the basement-cover contact (Fig. 5). Here, auriferous quartz-vein sets are spatially closely associated with tightly folded (F2b) horizons of siliceous slate, quartzite and mafic sills.

4.2. Gold mineralization along the basement-cover detachment

4.2.1. Fluid alteration

Regional-scale, syn-tectonic (D2) fluid flow and alteration in rocks below and above the basement-cover contact (e.g. Fig. 7a and b) are indicated by a number of features (e.g. Koegelenberg and Kisters, 2014; Koegelenberg et al., 2015). Pervasive quartz veining attests to fluid flow both in footwall gneisses and the detachment zones (Fig. 7c). Based on cross-cutting relationships and relative deformation, several generations of quartz veins can be distinguished (see Section 4.2.2 and 4.2.3). In places, quartz veins form up to 50 m thick and 550 m long lens-like quartz blows along the basement-cover detachment. The brecciation of quartz-blows and multiple quartz-vein generations indicate

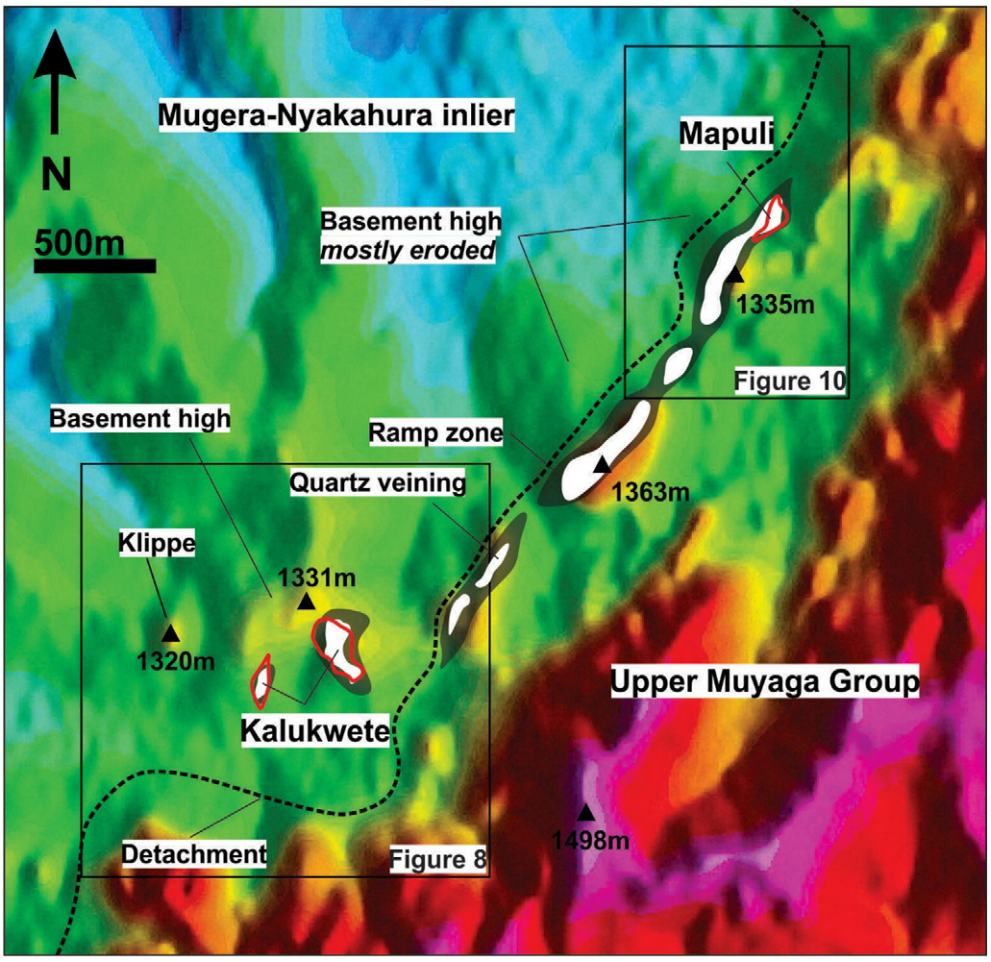

Fig. 5. Regional digital terrain model (DTM) of the detachment and artisanal mines with inferred basement ramp zones and significant quartz veining.

the multiphase reactivation of fluid conduits and protracted duration of the fluid flow. Muscovite-chlorite phyllonites (Fig. 6b) in the detachment are derived from the hydration of mainly quartzofeldspathic basement gneisses associated (Fig. 6a) with this fluid flow and quartz veining. The hydration is associated with the syn-D2 pyritization of the rocks, although primary sulphides are only very locally preserved and, for the most part, pseudomorphed by iron hydroxides (Fig. 6a, b, c, d, f).

In the hanging wall intensely deformed graphitic schists of the Upper Muyaga Group are likewise characterized by pervasive sericitization, abitization, secondary Fe oxides and pyrite (pseudomorphed by limonite and hematite) along foliation- and bedding planes and quartz veins (Fig. 6e, f). Schists with a high graphite content in close proximity to the detachment are particularly laced with pyrite and contain single pyrite minerals of up to 6 cm in diameter (Fig. 6f). Euhedral pyrite is syntectonic and has grown during the formation of the S2 foliation in the detachment, as the high strain S2 fabric in metapelites can be seen to be both deflected and overgrown by pyrite. Quartz strain shadows around pyrite grains are also common.

4.2.2. Kalukwete

4.2.2.1. Site description. Artisanal mining at Kalukwete has been active for several years. Mining is concentrated in a NNE-trending 4 km long and up to 800 m wide corridor parallel to the basement-cover interface. Gold mining is entirely in former basement gneisses that have been pervasively retrogressed to quartz-sericite-chlorite schists immediately below the main D2 detachment (Fig. 8). Mining in the mineralized part of the corridor at Kalukwete targets in-situ auriferous quartz veins and vein stockworks as well as alluvial gravel consisting of up to boulder sized vein quartz. In-situ workings are hosted by zones of near-pervasive sericitization of the wall rock gneisses (Figs. 6a, 9b). The workings expose the gradual increase in sericitization, ferruginization, from the weathering of original sulphides, and fabric intensities from weakly altered footwall gneisses to pervasively retrogressed and pervasively foliated phyllonites that constitute the actual detachment. Original quartz vein geometries and overprinting relationships are best developed in the footwall and some 5–20 m below the detachment. Quartz veins become progressively transposed and, in the process, brecciated and overprinted in the high-strain basement-cover detachment.

4.2.2.2. Quartz veining. Cross-cutting relationships of quartz veins in exploration pits and on a regional scale (Fig. 9a) indicate up to five distinct generations of veining. The earliest veins seem to pre-date D2 strains and are possibly associated with earlier Archaean- and/or Paleoproterozoic events bordering the TC. However, given their geometry and structural position, most veins can be related to progressive D2 strains and top-to-the NW and W kinematics along the detachment at various stages.

Set 1 and 2-(early pre-D2) veins: Set 1 veins are the earliest and are transposed, isoclinally folded and often rootless within the regional basement gneissosity. Set 2 veins are later, cross-cutting, orientated either parallel or at low angles to the pre-D2 gneissosity. Both sets of veins show mostly NNE trends and are associated with pre-D2 mylonite bands into which they are either transposed (set 1) or emplaced (set 2). The mainly massive, smoky- to milky white,

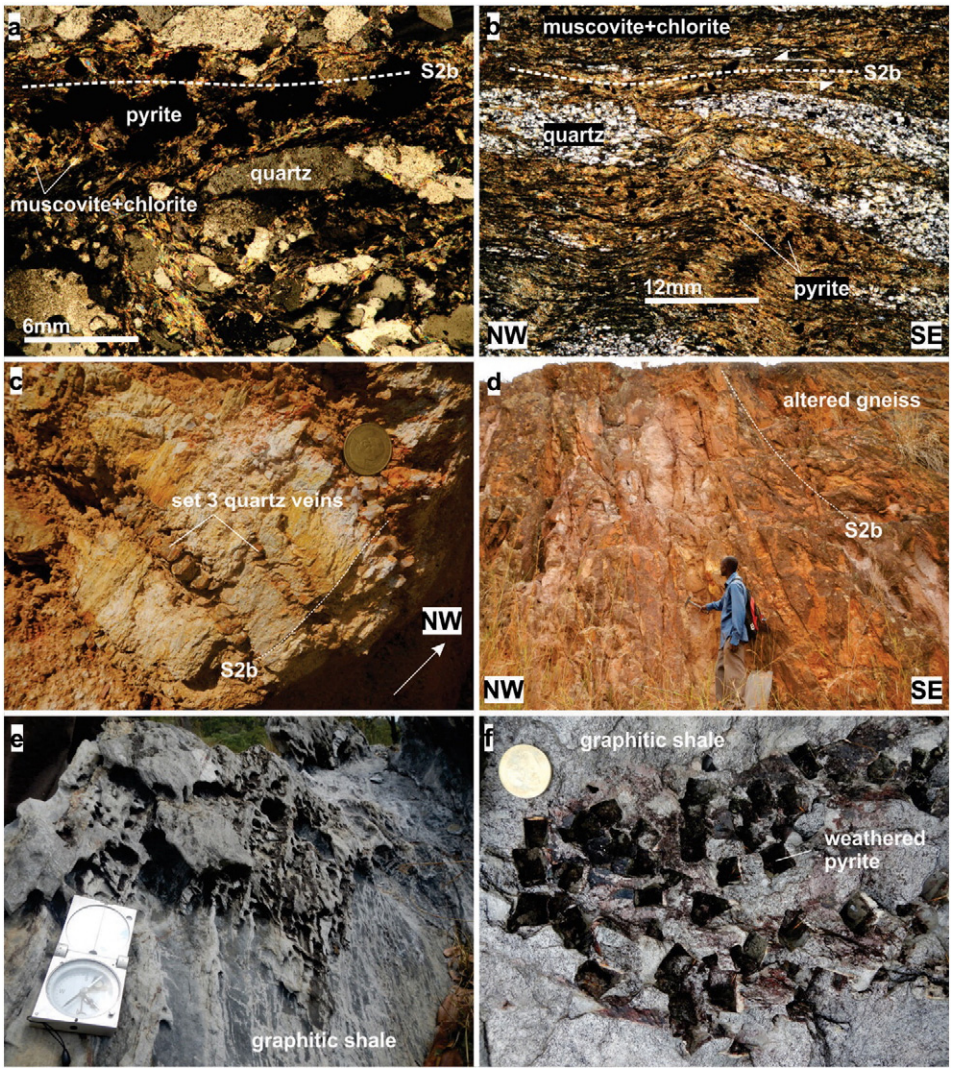

Fig. 6. a) Mica bearing shear band in gneiss with abundant pyrite. b) Intensely foliated and fully developed phyllonite with re-crystallized quartz lenses and pyrite showing weak top-to-the-NW S-C fabrics. c) Sericitized feldspathic gneiss with pervasive set 3 shear quartz veins. d) Highly altered gneiss exposed in quarry showing pervasive limonite and hematite staining. e) Graphitic slate/schist with pervasive hydraulic fracture network and associated abitization, sericitization and pyritization. f) Late-tectonic large, almost euhedral, pyrite pseudomorphs in graphitic shale.

quartz veins are lensoid and commonly brecciated. Vein thicknesses range from several millimetre thick veinlets to 80 cm thick veins, the latter of which can be traced for up to 80 m along strike. Notably, Set 1 and 2 veins are intersected in boreholes to depths of up to at least 150 m, underlining the probably pre-D2 origin and forming part of earlier events that have affected the basement gneisses.

Set 3 - D2 shear veins: Set 3 veins cross-cut both fabrics in basement gneisses and earlier quartz vein generations (Figs. 6a, 9a, d) and are the dominant vein set in the workings. Offsets of fabrics and earlier vein sets across set 3 veins indicate the veins are shear veins. Set 3 veins show predominantly NE strikes with moderate to steep dips to the NW. Vein thicknesses vary between ca. 0.02–1.5 m and the thickest veins can be traced for several hundred meters along strike (Fig. 8). At depth, the veins become thinner and pinch out altogether at ca. 30–40 m into the footwall, whereas thicknesses are at a maximum in sericitized gneisses below the detachment. Most veins are brecciated and consist of milky- to light smoky quartz. Numerous set 3 veins contain fragments of earlier dark smoky quartz, similar to that from set 1 and 2 veins, and wall-rock gneisses.

Set 4 - D2 lenticular veins: Set 4 veins are orientated sub-parallel with S2b phyllonites of the detachment. The milky white veins are invariably deformed and lensoidal, between 2 cm and 30 cm thick, and brecciated and/or boudinaged. Most set 4 veins are strongly ferruginous, indicating the abundance of former sulphides (Fig. 9c). Multiple and renewed veining is evident in many of the set 4 veins. The absolute timing of set 4 veins is not unambiguous and many of the veins may form part of set 3 veins that have been caught up and transposed into the high-strain fabrics of the D2 detachment.

Set 5 - Late D2 extension veins: Late D2 tension veins are developed as highly ferruginous 2 to 5 mm thin quartz veins and brecciated quartz veins that cut the phyllonites of the detachment at high angles (Fig. 9f). These veins are mostly developed in thick veins of earlier quartz vein generations (set 1 and 2 veins) or stockworks of earlier vein sets (set 3 and 4 veins). The occurrence of these latest stage veins seem largely restricted to shallow depths below the main D2 detachment not exceeding 25 m.

4.2.2.3. Mineralization. Gold mineralization to depths ca. 20 m below the basement-cover detachment is associated with predominantly set 3 veins. Closer to the detachment, late set 5 tension veins become

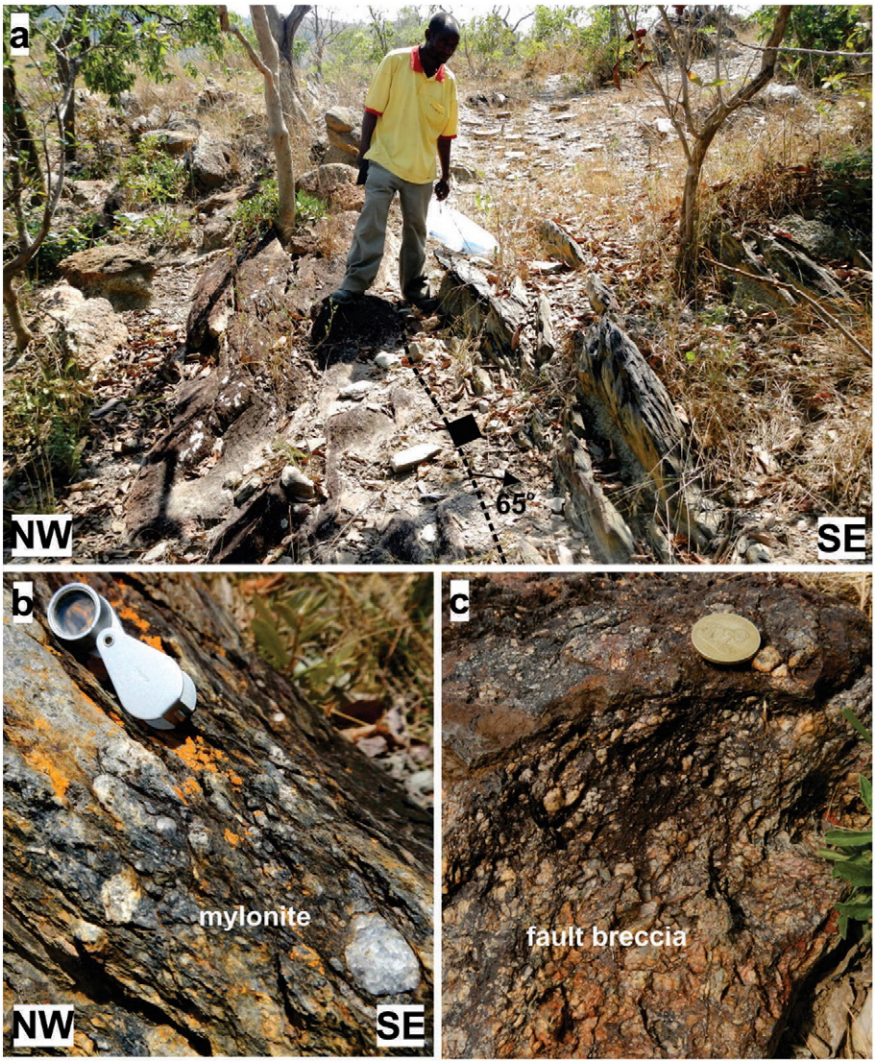

Fig. 7. a) Steep SE dipping contact between altered gneiss and graphitic schist. b) Thick mylonite along detachment in graphitic shale with competent clasts of quartz vein and quartzite. c) Highly ferruginous and siliceous fault breccia at basement-cover contact consisting of mostly fractured quartz vein clasts.

increasingly abundant and are the main mineralized set. Mineralized quartz veins are almost invariably ferruginous containing abundant limonite and/or hematite, whereas original sulphides, mainly pyrite, are only rarely preserved in the deep weathering profile. Gold occurs as up to 5 mm large specks of free gold particularly in brecciated set 3 veins (Fig. 9d, e). Specks of free gold also occur in thin late-stage set 5 veins (Fig. 9f). The majority of the auriferous set 5 veins seems confined to larger quartz blows of earlier set 3 veins and, to a lesser extent, in quartz blows of early set 1 and 2 veins.

The NE trending mineralized corridor at Kalukwete corresponds to undulations of the D2 detachment centred around a prominent basement high (Fig. 5). On average, the detachment shows shallow (ca. <10°) dips to the southeast and east below the structurally overlying Muyaga Group rocks along the eastern margin of the MN-inlier. However, the detachment surface is not smooth and segmented by distinct flat- and- ramp structures. The NE-trending undulations correspond to frontal ramps during top-to-the-NW kinematic transport along the detachment. Local contacts and S2b foliations indicate that flats are characterized by shallow NW or sub-horizontal dips, whereas ramps show SE dips at dip angles of between ca. 20° and 30° (Fig. 8). This undulating geometry is underlined by a high-resolution digital terrain model (DTM) that outlines undulations of up to 30 m in the basement-cover contact around the Kalukwete mining camp (Fig. 5, see also outline on Fig. 3). Considering alluvial overburden covering much of the contact and partial erosion of the basement, the extent of the ramps, as well as dips, are likely to be underestimates. Spatially mineralized set 3 and set 5 shear- and late extensional veins are preferentially developed on ramps that define the eastern slope of the basement high, whereas the western slope of the basement high is not mined (Fig. 5).

4.2.3. Mapuli

4.2.3.1. Site description. The Mapuli prospect is located directly above the basement-cover detachment in folded graphitic schist of the Upper Muyaga Group (Fig. 10), some 3 km north of Kalukwete. Mining is confined to within a ca. 50 m thick ridge of massive milky and partly brecciated quartz that can be followed for ca. 2 km along the basement-cover contact directly below the Muyaga Group graphitic schists derived from original slates (Fig. 11a). F2b folds in the schists show NNE trends and shallow plunges and a prominent NW vergence, corresponding to the overall top-to-the-NW kinematics recorded along the basement-cover detachment. Smaller-scale top-to-the-NW thrusts (D2b) in the sequence are defined by 1–50 cm thick phyllonite and/or mylonite bands localized in incompetent graphitic schists.

4.2.3.2. Quartz veining. In contrast to Kalukwete, Mapuli is characterized by a rather massive silicification and up to 50 m thick quartz-vein blows along the basement-cover contact. The sheer volume of quartz makes a distinction of individual quartz vein generations difficult, but there is clear evidence for the multiple reactivation and brecciation of larger quartz blows by younger quartz-vein sets (e.g. Fig. 11a). At Mapuli the transposition of quartz veins along the basement-cover interface is preserved in graphitic schists of the Upper Muyaga Group. Earlier set 1 and 2 vein sets are absent, but later vein sets, similar to those at Kalukwete are evidenced by cross-cutting relationships and their orientation.

Set 3 - D2 shear veins: Set 3 veins appear to be the most abundant at Mapuli and are predominantly massive, consisting of distinctive milky white quartz containing angular fragments of graphitic schist (Fig. 11b), granite (gneiss) and dark smoky quartz (set 1, 2). In parts set 3 veins have been brecciated by later quartz veins. Individual shear veins are up to 2 m thick and strike NE to NNE with steep dips (50°–75°) predominantly towards the NW. These vein sets are at moderate to high angles (ca. 60°) with the principal direction of shortening, as indicated by dominant S2b foliations (Fig. 11c).

Set 5 - Late D2 extension veins: Set 5 tension veins are between 2 mm and 15 cm thick and are particularly prominent at the Mapuli mine. The late-stage veins are confined to earlier formed massive quartz veins created by the close spacing and clustering of multiple set 3 shear quartz veins (Fig. 11d). Two nearly sub-horizontal geometries can be distinguished including moderately (5°–20°) SW and NE dipping veins. The sub-horizontal dip of set 5 veins indicates an origin as extensional veins that formed during regional sub-horizontal shortening (D2). Set 5 veins are mostly filled with yellow to dark red oxidized massive hematite, limonite and goethite, and vein quartz breccia.

4.2.3.3. Mineralization. Mining at Mapuli targets disseminated gold concentrated predominantly in late set 5 extensional veins characterized by abundant Fe oxides (Fig. 11d, e). The auriferous veins are confined to the earlier formed massive and brecciated quartz blows along the basement-cover contact made up of numerous overprinting and amalgamated Set 3 veins. Extension veins are pervasive throughout quartz blows and form narrow clusters with a spacing of between 20 cm to 2 m. Mining follow the prominent clusters and/or thick single veins, but also alluvial gravel down slope.

The silicification and subsequent formation of late mineralized quartz blows at Mapuli is localized and can be traced southwards along the detachment for some ca. 2–3 km, indicated by prominent quartz ridges. Here the detachment corresponds with more steeply south-east dipping basement-cover contacts of up to 35–45° (Fig. 10). These ramp structures spatially coincide with the voluminous, elongate quartz blows. In contrast, localized ramp contacts with dips steeper than 60° show (Fig. 7a) significantly less silicification and are not mined.

5. Mine operations in the Muyaga Group

5.1. Mtakuja

5.1.1. Site description

Mtakuja is located stratigraphically higher up in rocks of the Muyaga Group some ca. 2 km east of the basement-cover detachment and at least ca. 300–400 m above the basal D2 detachment (Figs. 3, 12, 13a). Mining operations can be followed along a prominent ridge structure for some 0.3 km and parallel to the NNE strike of the folded Muyaga Group. Mining mainly targets in-situ auriferous quartz veins, but also alluvial and a structurally higher ferricrete paleo-horizon forming the top of the ridge.

The area is underlain mainly by slates of the Muyaga Group and isolated interlayered quartzites and intrusive sills. The mining operations are located in the hinge of a shallow (5–10°) NNE-plunging, NW-verging, tight and overturned F2b anticline with a wavelength of ca. 0.4 km (Fig. 12). The limbs of the F2b anticline are delineated by an up to 3 m thick marker horizon of quartzite, while the core of the fold consists of predominantly interlayered pink and white siliceous slate

Table 1
O-isotope results and sample descriptions. Notes: All quartz analysed by laser fluorination, all whole rock samples by conventional fluorination. All $\delta^{18}O$ values reported relative to SMOW (see text).

Sample	$\delta^{18}O$ (‰)	Type	Location	Description
Basement – detachment footwall				
B5	8.2	Quartz vein	Kalukwete	(Pre-D2), set 2 - shear vein
B6	10.0	Quartz vein	Kalukwete	(Pre-D2), set 2 - shear vein
D3	9.7	Quartz vein	Kalukwete	Early Pre-D2, set 1 - transposed vein
B7	11.4	Quartz vein	Kalukwete	Set 3 - shear vein, Au mineralized
B9	11.9	Quartz vein	Kalukwete	Set 3 - shear vein, Au mineralized
B8	12.9	Quartz vein	Kalukwete	Set 3 - shear vein, Au mineralized
B2	10.4	Whole rock	Kalukwete	Cataclastic textured biotite gneiss (Pre-D2)
B3	10.9	Whole rock	Kalukwete	Granite with moderate sericite alteration
D2	11.1	Whole rock	Kalukwete	Muscovite schist (granite protolith)
B4	12.0	Whole rock	Kalukwete	Biotite gneiss with pervasive sericite alteration
B1	8.7	Whole rock	Kalukwete	Biotite granite (no alteration)
D1	8.1	Whole rock	Kalukwete	Mylonite (Pre-D2)
Cover – detachment hanging wall				
C6a	16.1	Quartz vein	Mapuli	Set 3 - shear vein, Au mineralized
C7a	16.4	Quartz vein	Mapuli	Set 3 - shear vein, Au mineralized
C6b	16.1	Whole rock	Mapuli	Highly graphitic schist
C7b	14.3	Whole rock	Mtakuja	Highly graphitic slate
C1	16.1	Quartz vein	Mtakuja	Massive A–C vein
C5	12.7	Quartz vein	Mtakuja	A–B vein, Au mineralized
C4	12.4	Quartz vein	Mtakuja	A–B vein, Au mineralized
C8	14.8	Quartz vein	Mtakuja	Set 3 - shear vein
C9	13.8	Quartz vein	Mtakuja	Massive A–C vein
C2	14.8	Whole rock	Mtakuja	Ortho-quartzite
C3	12.4	Whole rock	Mtakuja	Micaceous and siliceous slate
C8	8.1	Whole rock	Mtakuja	Metamorphosed mafic sill (minor alteration)
C9	12.8	Whole rock	Mtakuja	Metamorphosed mafic sill (altered)
C11	16.0	Whole rock	Mtakuja	Metamorphosed mafic sill (highly altered)

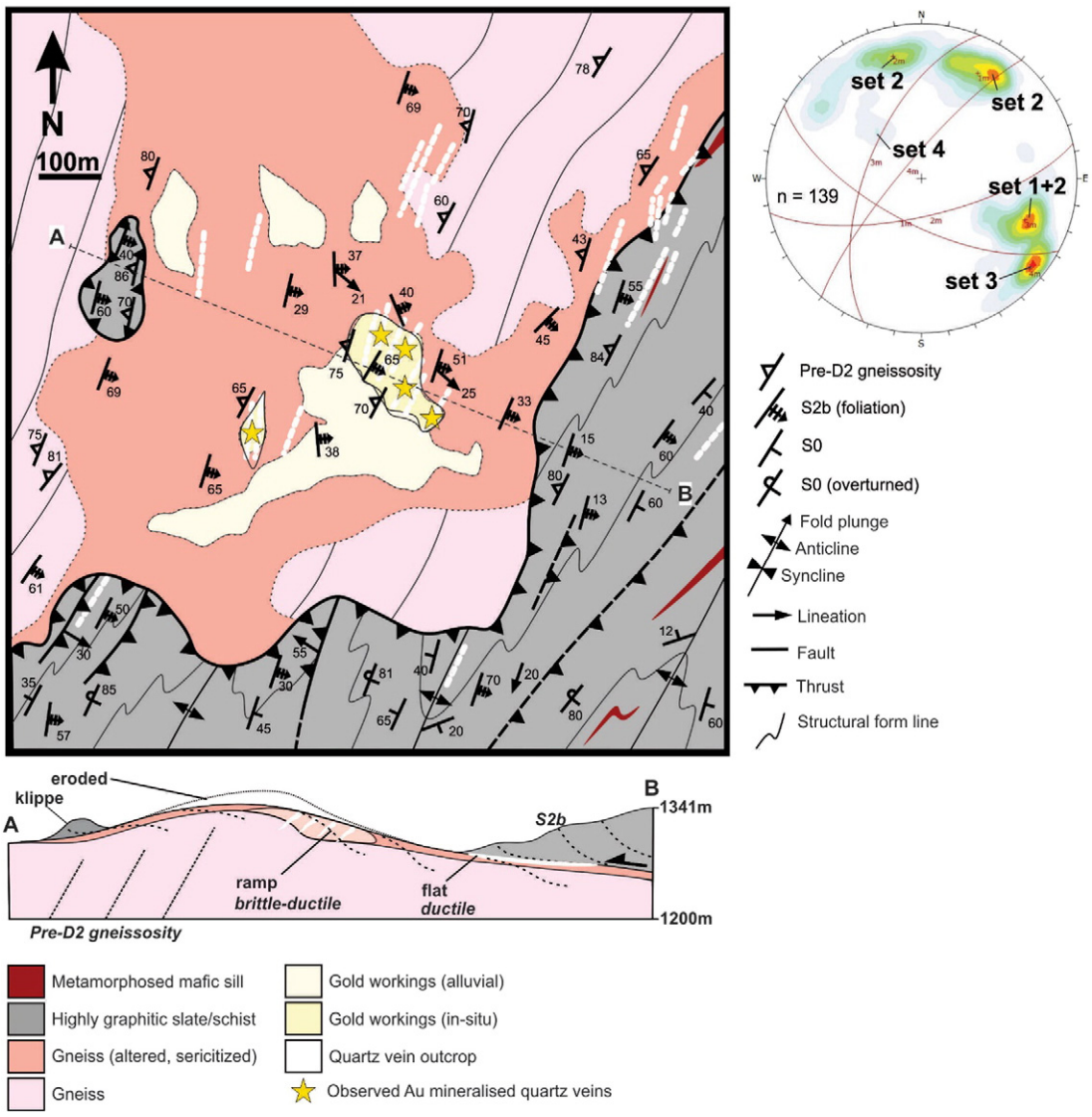

Fig. 8. Geological map of Kalukwete and surrounding country rock including a cross section (A–B). Dominant quartz vein geometries are shown as contours of poles-to-plane points on a lower hemisphere, equal area, stereonet.

and arkose, and lesser graphitic slate. Importantly, an up to 5 m thick mafic, but pervasively altered and strongly ferruginous, dolerite sill forms part of the folded sequence and has been duplicated in the hinge of the anticline. This folded sill is laterally extensive and can be traced along strike for several tens of kilometres to the north and south of Mtakuja.

5.1.2. Quartz veins

Silicification and quartz veining at Mtakuja are almost solely concentrated in and around the tightly folded quartzite bed (Fig. 13b) and mafic sill. Both bedding-parallel and cross-cutting vein geometries are developed that indicate a focused, structurally and lithologically controlled fluid flow. Incompetent slate layers show significantly lower quartz-vein abundances and densities compared to the central quartzite bed and mafic sill. Late quartz vein sets (see below) are transgressive through most lithotypes, but generally pinch out in slate. Distinct quartz-vein sets confined to the central quartzite unit and mafic sill include:

Bedding parallel- and ladder veins: Bedding-parallel veins predominantly extend along bedding contacts between quartzite or the central mafic sill and arkose (Fig. 13c). Vein thicknesses on the fold limbs are ca. 20 cm, but can increase up to 45 cm in the crests of parasitic F2b folds. In the first-order F2b fold bedding-parallel veins can be continuous for >200 m along strike. The veins are predominantly massive and consist of light grey- and milky quartz, with subordinate iron oxides. On fold limbs, veins may be brecciated and cemented by later-generation vein quartz.

Ladder veins are transgressive through competent quartzite beds and the dolerite sill, orientated at high angles to bedding planes or intrusive contacts, but are connected with bedding-parallel veins. Ladder veins range in thickness between 2 and 15 cm. They are extensional veins that follow tension fractures on limbs and/or radial fanning joints in fold hinges. For the most part, ladder veins appear relatively unreformed, indicating a relatively late timing during folding.

Conjugate shear veins: Conjugate shear veins (Fig. 13b) constitute a volumetrically subordinate vein set orientated at high angles to the steeply dipping bedding on fold limbs of second-order F2b folds. The veins cross-cut bedding and form single planar shear fractures or en-echelon arrays. Individual veins are up to 10 cm thick whereas veins in en-echelon vein arrays are much thinner, not exceeding

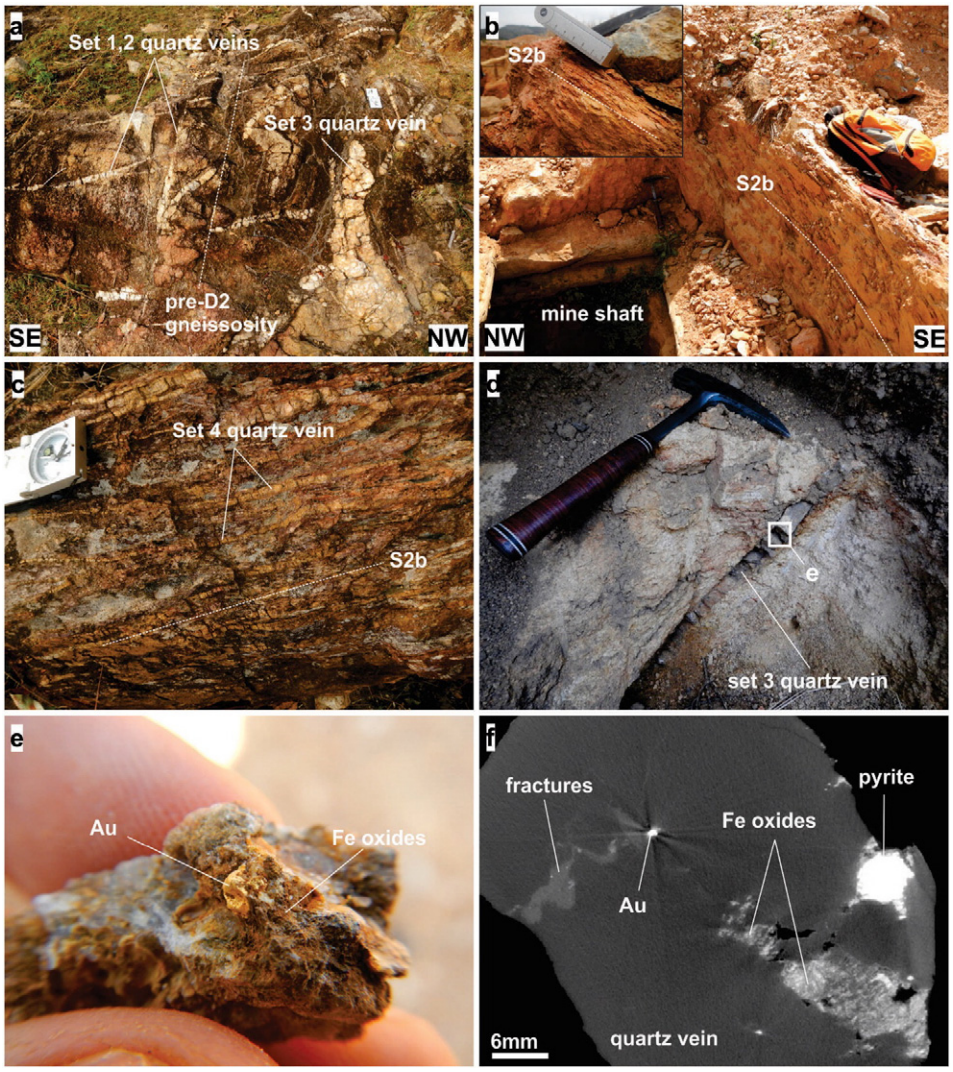

Fig. 9. a) Gneiss pavement showing clear cross-cutting relationship between early pre-D2 (set 1, 2) and D2 (set 3) quartz veins. b) A shallow mine shaft within transposed and highly foliated (S2b) altered gneiss. c) Intensely strained phyllonites laced with mylonite bands and associated lenticular quartz veins along the detachment. d) Mining of fractured mineralized set 3 shear vein. e) A cluster of a set 3 shear vein with specs of disseminated gold, limonite and massive hematite in fractures. f) Nano CAT (computerized axial tomography) scan image of a set 3 shear vein cluster highlighting variable material densities. Note disseminated gold is indicated by very dense anomalies (bright white) that are associated with pyrite and other Fe-oxides (light to medium grey) following late set 5 fractures.

1 cm in thickness. Veins consist mostly of milky quartz with minor pyrite and iron oxides.

A–C veins: The term A–C quartz veins (Fig. 13b, d, e) highlights the orientation of this vein set at high-angles to the shallow NNE plunge of the F2b host anticline. AC veins are planar, subvertical, striking WNW and at high angles to the regional NNE F2b fold-axial trend. Cross-cutting relationships show A-C veins cross-cutting bedding-parallel-, ladder- and shear veins (Fig. 13b). The veins are gently deformed, with thicknesses between ca. 5–35 cm, and consist of massively textured milky quartz and only little iron oxides and hydroxides.

A–B veins: A–B quartz veins (Fig. 13b, f) are the latest quartz vein set that cross-cut all other quartz-vein generations. The veins are sub-horizontal to shallow (10°–23°) WSW to ENE dipping veins that are orientated at high angles to the regional axial planar S2b fabric. The veins are most abundant in F2b fold hinges where they are gently buckled. The veins cross-cut competent quartzites and the mafic sill, but are also developed in less competent slate and arkoses. Vein thicknesses vary between 0.2 and 2 cm in slate and up to 8–10 cm in the dolerite sill. The vein quartz has a distinct white to smoky colour with fractured blocky textures and abundant iron oxides.

5.1.3. Mineralization

Mining operations closely follow quartz veins in the highly altered and metamorphosed mafic sill and micaceous wall rock arkoses and slates laced with hematite and limonite pseudomorphs after pyrite. Late-stage B–C veins transecting the mafic sill and immediate wall rocks are the main target of the artisanal mining and contain abundant Fe-oxides and disseminated gold. Structurally late B–C quartz veins are preferentially developed within the anticlinal hinge zone of the host F2b fold (Fig. 12). The overall spatial distribution of disseminated Au along the margins- or within highly altered mafic wall rock implicates an additional chemical control to mineralization.

6. Oxygen isotopes

6.1. Sampling and analysis

A total of 13 whole-rock and 13 quartz-vein samples were analysed for oxygen isotopes (Table 1) in order to constrain potential fluid

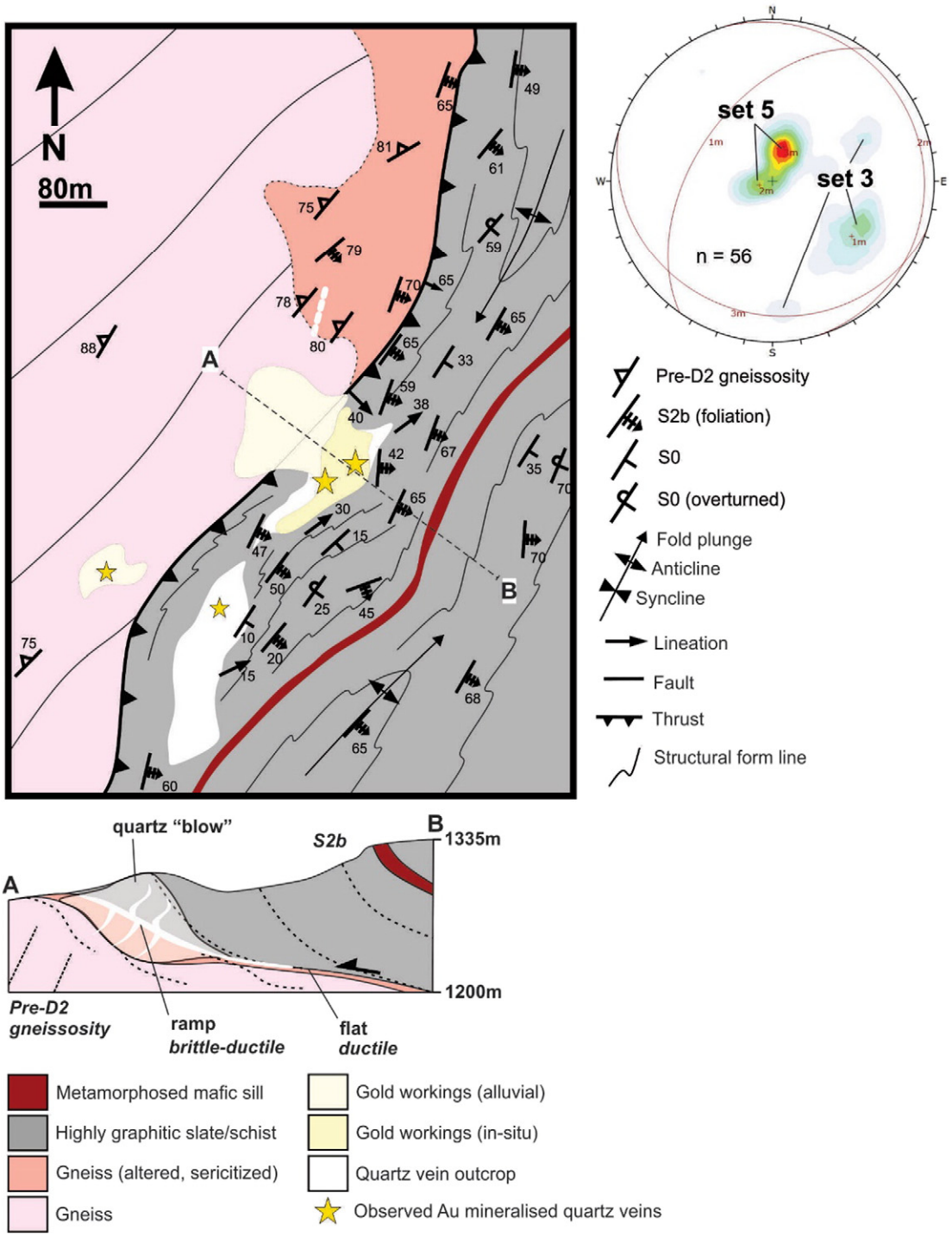

Fig. 10. Geological map of Mapuli and surrounding country rock including a cross section (A–B). Dominant quartz vein geometries are shown as contours of poles-to-plane points on a lower hemisphere, equal area, stereonet.

sources of the regional alteration and mineralization. The relative stratigraphic position of whole-rock samples are shown in Fig. 4.

For oxygen isotopes, both conventional and laser fluorination methods were used. Whole-rock powders were analysed using a conventional silicate line following methods described by Harris and Ashwal (2002). Approximately 10 mg of sample was reacted with ClF_3, and the liberated O_2 converted to CO_2 using a hot platinized carbon rod. Quartz vein material was analysed by the laser fluorination method described by Harris and Vogeli (2010). In some cases, single pieces were analysed, in others multiple pieces were analysed. All samples were pre-fluorinated overnight, where after each 1–3 mg sample was reacted in the presence of approximately 10 kPa BrF_5, and the purified O_2 was collected onto a 5 Å molecular sieve contained in a glass storage bottle.

All O-isotope ratios were measured off-line using a Finnigan Delta XP mass spectrometer in dual-inlet mode on either CO_2 (conventional) or O_2 (laser) gas. All data are reported in δ notation where $\delta^{18}O = (Rsample / Rstandard - 1) * 1000$, and R = the measured $^{18}O/^{16}O$ ratio. For the whole-rock data, duplicate splits of the quartz standard (MQ) were run with each batch of eight samples, and were used to convert the raw data to the SMOW scale using the $\delta^{18}O$ value of 10.1% for MQ. The long-term variability of MQ suggests a 2σ error of 0.16‰. For the laser fluorination analyses, two splits of our internal standard

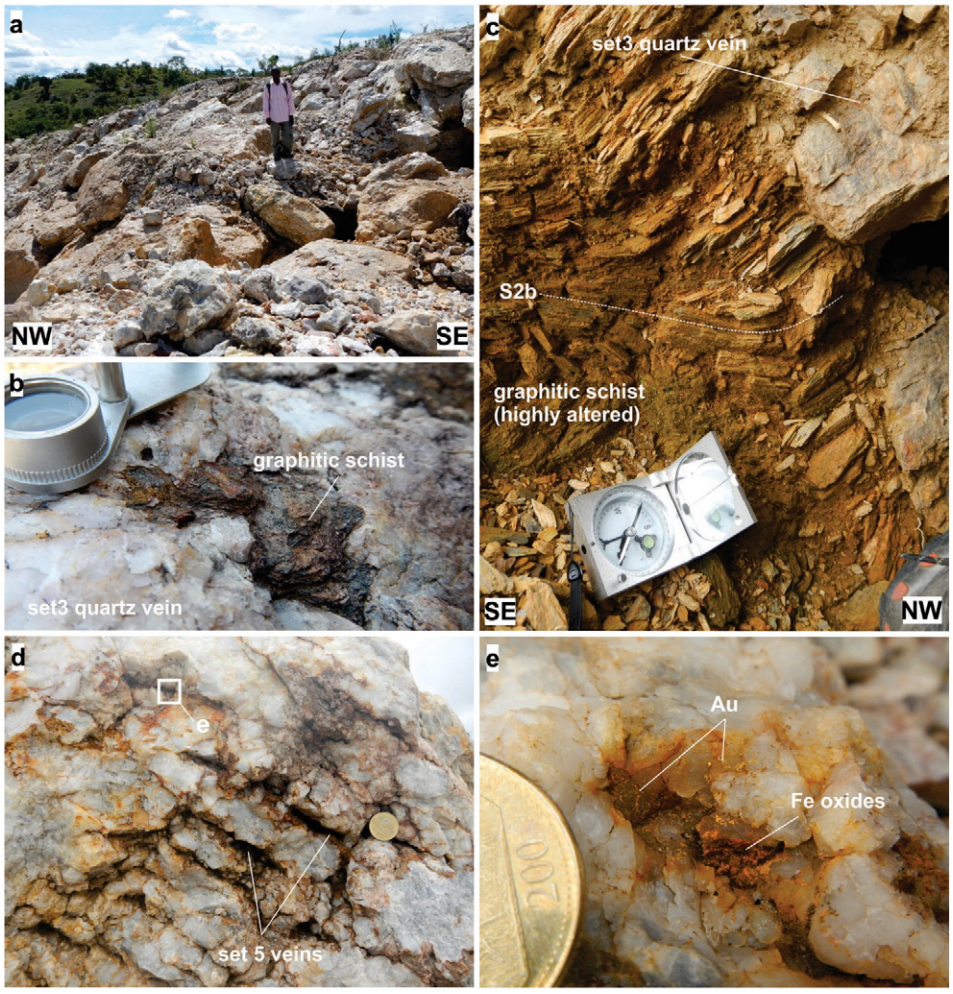

Fig. 11. a) Extensive mine workings at Mapuli targeting massive quartz "blows". b) Clast of graphitic schist (Upper Muyaga Group) in set 3 shear quartz vein. c) Set 3 shear quartz vein cross-cutting intensely S2b foliated graphitic schists. Note slight rotation of S2b indicating slight reverse top-to-the-SE slip along fracture plane. d) Cluster of closely spaced set 5, sub-horizontal, extensional veins/fractures. e) Close view of an open set 5 extensional fracture showing limonite and disseminated specs of gold.

MON GT (5.38‰, Harris and Vogeli, 2010) were analysed with each batch of 10 samples. The long-term average difference in $\delta^{18}O$ values of duplicates of MON GT is 0.12‰, which corresponds to a 2σ value of 0.15‰ (n = 185). San Carlos olivine grains were also analysed during the course of this work and gave an average $\delta^{18}O$ value of 5.33‰ (±0.32‰, 2σ n = 9) which is comparable to the $\delta^{18}O$ values of 5.35‰ reported by Eiler et al. (2011). Yields were measured for all conventional analyses by means of a small volume cold finger and a pressure transducer during the extraction procedure. For quartz analysed by laser fluorination, the yield was determined by measuring the pressure of gas in the mass spectrometer inlet at constant volume. In all cases, the yields were close to the expected 100% yield based on the weight of sample.

6.2. O-isotope results

Pre-D2 quartz veins from basement gneisses at Kalukwete have $\delta^{18}O$ values (Table 1) between 8.2 and 10.0‰ (B5, B6, D3), whereas quartz veins associated with D2 deformation, and the regional detachment, range from 11.4–12.9‰ (B7, B8, B9). Similarly, host basement rocks with the least amount of retrogression record $\delta^{18}O$ values of 8.1–8.7‰ (B1, D1), while moderately retrogressed gneisses range from 10.4–12.0‰ (B2, B3, D2, B4).

Quartz veins from Mapuli, which is situated in graphitic schists (previously slate) of the Upper Muyaga Group and also associated with the regional D2 detachment, have markedly higher $\delta^{18}O$ values of 16.1–16.4‰ (B5, B6). These values are similar to those of the host graphitic schists which have $\delta^{18}O$ value of 16.1‰ (C6b).

Quartz veins from Mtakuja, by comparison with Mapuli, have more variable $\delta^{18}O$ values ranging from 13.8–16.1‰ (C1, C8, C9) and 12.4–12.7‰ (C4, C5). Host rocks of slate and quartzite have $\delta^{18}O$ values of 14.3–14.8‰ (C2, C7b), whereas mafic sills have $\delta^{18}O$ values of 8.1 and 12.1‰ (C8, C9). Lastly, an extremely altered part of the mafic sill (C11) has a $\delta^{18}O$ value of 16.0‰.

7. Discussion

7.1. D2 fluid flow along the detachment

Pervasive alteration, silicification and syntectonic (D2) pyritization delineates the sheared basement-cover contact around the MN inlier as a narrow, but regionally extensive zone where fluid flow has occurred. Fluid flow and alteration have affected both the sheared detachment rocks and wall-rocks below and above the basement-cover contact (e.g. Koegelenberg and Kisters, 2014). The main D2 detachment combines a number of characteristics of low-angle faults. Voluminous quartz veining and overprinting vein generations indicate episodically close-to-lithostatic fluid pressures and fluid pressure cycling along the detachment. Elevated fluid pressures contribute to a lowering of the effective stress and facilitate reactivation and slip along the shallowly-dipping fault. Fluid flow and associated alteration have, in turn, led to the formation of mica-dominated phyllonites. This

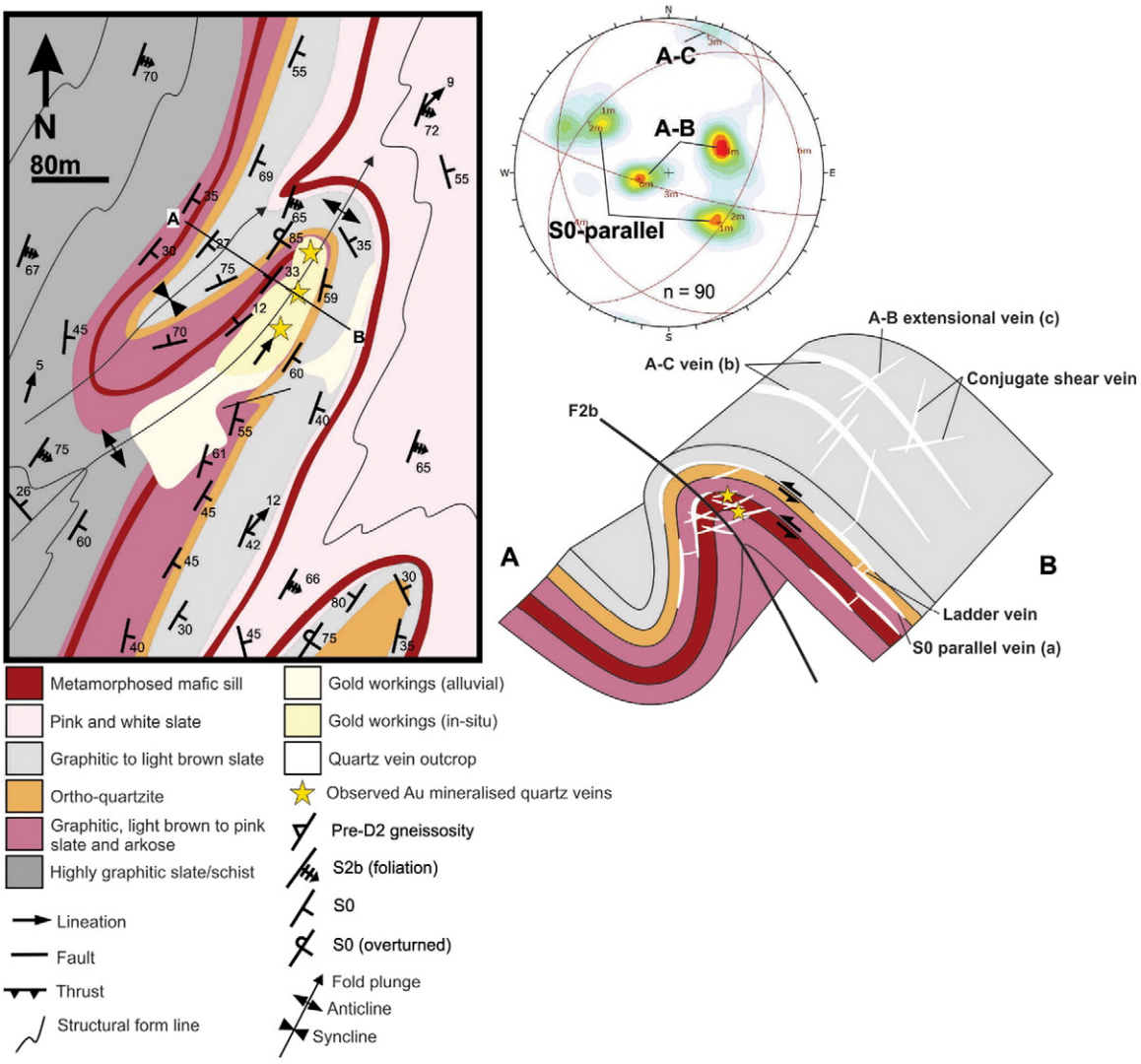

Fig. 12. Geological map of Mtakuja and surrounding country rock including a schematic 3D cross section (A–B) with quartz vein geometries. Dominant quartz vein geometries are shown as contours of poles-to-plane points on a lower hemisphere, equal area, stereonet.

reaction weakening further weakens large parts of the D2 detachment. Quartz-vein stockworks immediately below the detachment document the competence contrast between the weak detachment rocks and the much stronger quartzo-feldspathic gneisses. The vein networks suggest that ductile, aseismic creep in the low-cohesion detachment was accommodated by episodic brittle fracturing and quartz veining in the footwall gneisses. This relationship between fault slip and quartz veining is underlined by the decrease of quartz veins at depth and with greater distance from the upper detachment. Syn-D2 quartz-vein sets are not developed at depths > 25 m below the detachment where only older vein sets 1 and 2 are present. The syn-kinematic (D2) timing of quartz veining is indicated by (1) the orientation of quartz vein sets (Set 3, 5), corresponding to extension- and shear fractures (Figs. 6c, 11d), and (2) the progressive rotation and transposition of veins in closer proximity to and within the detachment. In fact, much of the phyllonitic detachment has formed through the hydration of originally quartzo-feldspathic footwall gneisses rather than from schists of the overlying Muyaga Group. Hence, transposed and dismembered quartz veins in the detachment phyllonites are probably derived from earlier veining episodes in gneisses, recording the progressive hydration and downward widening of the detachment due to reaction weakening (retrogression) and subsequent strain softening.

Despite the regional extent of fluid flow, the localized occurrence of mineralized zones and mining operations suggest additional controls and the Kalukwete and Mapuli prospects demonstrate a case in point. Systematic changes in the dip of the basement-cover contact describe an undulating detachment geometry in which NE-trending ramp-like structures with dips of ca. 30–35° alternate with flatter (5–10°) parts of the detachment (Figs. 8, 10). Mining at Kalukwete follows an intensely silicified zone that parallels a ramp-structure in the detachment (Fig. 5). Steep (>60°), frontal ramp structures correspond to misoriented faults, in the sense of Sibson et al. (1988), where the steeper dips result in increased shear resistance and strain accumulation. In contrast, ramp structures with dips closer to ca. 30° are more optimally orientated for fault slip in the regional D2 stress field ($\sigma 1$ horizontal; $\sigma 3$ vertical), assuming an ideally Anderssonian fault-type behaviour (Nguyen et al., 1998; Fagereng et al., 2014) (Fig. 15). This implies that fault slip along the ramps occurs at relatively lower shear stresses and optimally orientated ramps are likely to lead to the preferential nucleation of fault slip along the weak detachment and associated brittle failure and quartz veining in the competent footwall gneisses (Nguyen et al., 1998). It is this combination of repeated slip along two juxtaposed, mechanically contrasting lithotypes above and below the detachment that accounts for the localized pervasive quartz veining and mineralization at Kalukwete. (See Fig. 15.)

Mining at Mapuli, in contrast, focuses on massively silicified parts of the detachment. Silicification also follows NE-trending ramp structures with dip angles of up to 45° (Fig. 15). These ramp dips are steeper than

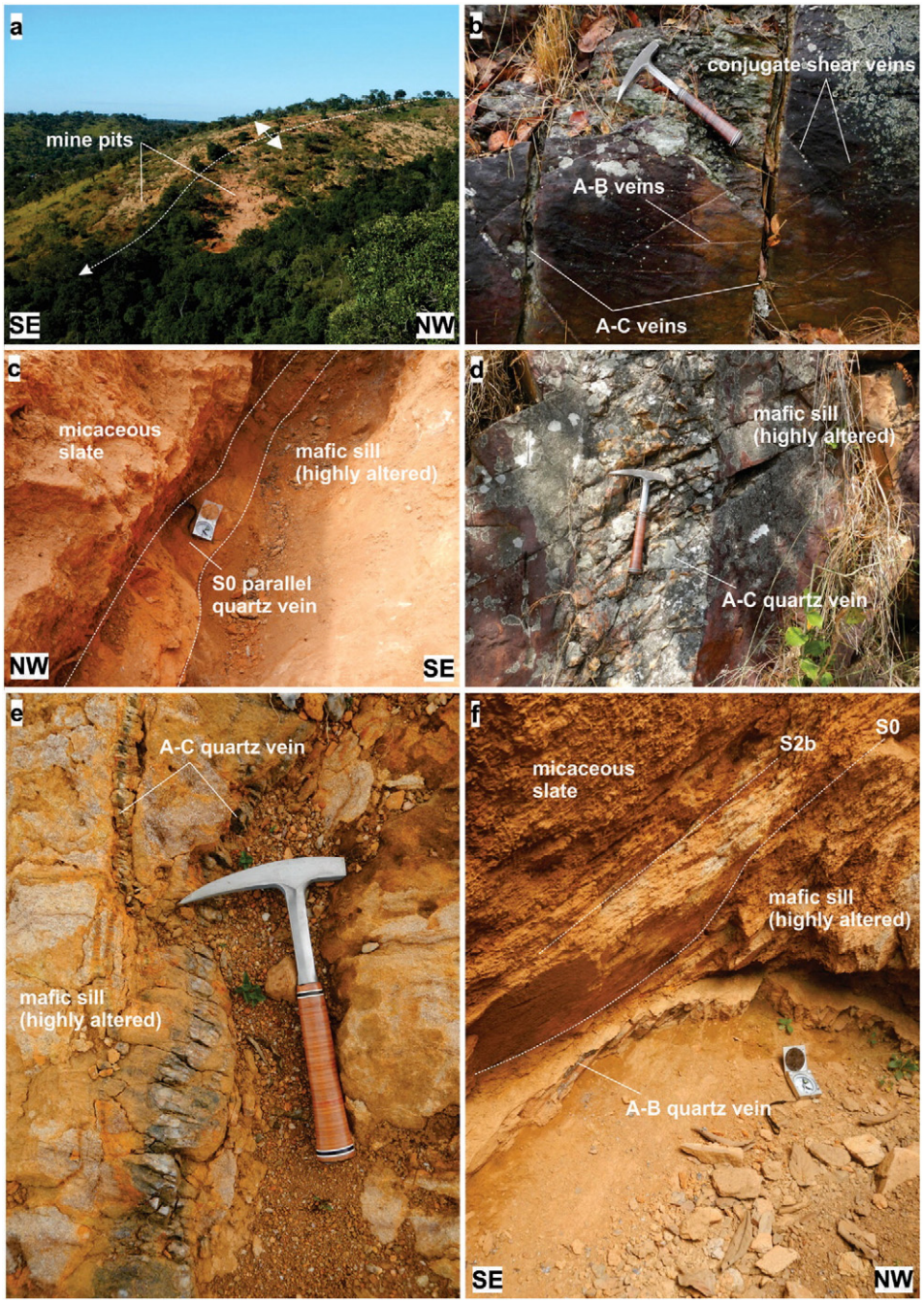

Fig. 13. a) View of Mtakuja and NNE plunging anticline. b) Quartzite on tight F2b fold limb showing cross-cutting relationships of dominant quartz vein sets. c) Thick bedding parallel quartz vein in contact with mafic sill. d) Thick sub-vertical A–C quartz vein cross-cutting competent mafic sill. e) Exposed gently folded A–C quartz veins in highly altered mafic sill in mine pit. f) Sub-horizontal and highly mineralized late B–C quartz vein partially cutting through an altered mafic sill and slate.

ramp structures at Kalukwete. The large and massive quartz blows form relatively competent inclusions along the detachment. This causes a steepening of the detachment as it wraps around the quartz blow. In this orientation, fault slip may be delayed and partially inhibited by increasing strain and shear resistance along the more steeply inclined detachment. Lock up of the detachment may instead favour fault-valve action and the formation of sub-horizontal extension fractures and associated fluid-pressure cycling, or seismic pumping (Sibson et al., 1988). Veins formed at this stage are represented by the sub-horizontal late-stage D2 extension veins (set 5) that are confined to earlier formed quartz blows immediately below the detachment.

The auriferous vein networks in basement gneisses below the main detachment highlight the role of strain-dependent permeability enhancement and veining along lithologically and mechanically contrasting rock types (e.g., Hodgson, 1989; Oliver et al., 2001). This has also been documented for numerous Archaean lode-gold deposits (e.g., Ojala et al., 1993; Duuring et al., 2001). Competence contrasts during deformation are particularly pronounced under greenschist-facies conditions, where the brittle-ductile contrasts between micaceous greenstones and feldspathic granitoids is most prominent. Under the regional lower-greenschist-facies conditions in the Biharamulo district, gold is likely to occur as an Au(HS)2-complex in the hydrothermal solution (e.g., Seward, 1973; Zhu et al., 2011). The stability of the gold complex depends, amongst other factors, on temperature, oxygen fugacity and pressure. Fracturing and veining in basement gneisses and the associated episodic fluid pressure drops may lead to a phase separation and

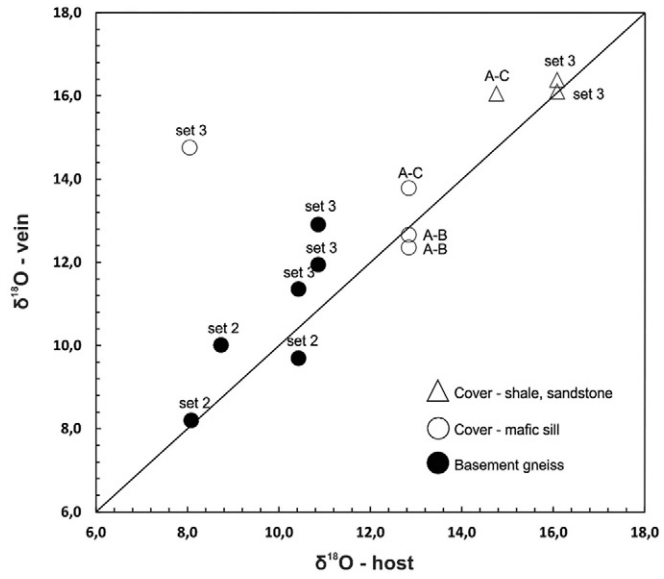

Fig. 14. XY scatter plot of $\delta^{18}O$ values for sampled quartz veins and associated wall rocks (host).

destabilization of the gold complex (Sibson and Scott, 1998). Given the chemically inert quartzo-feldspathic gneisses, fluid-pressure cycling is the most likely process that has triggered gold precipitation along the basement-cover interface.

7.2. D2 fluid flow in the Muyaga Group

Auriferous quartz veins and associated alteration at the Mtakuja prospect in the structurally overlying Muyaga Group demonstrates the regional scale of fluid flow. The D2 timing of this fluid flow is illustrated by the close spatial and temporal relationship between auriferous quartz veins and F2b folds and, specifically, competent and chemically reactive units during folding. Bedding-parallel and connecting shorter ladder veins document fluid infiltration and veining during the initial stages of folding, when flexural slip was operative during fold amplification. The late-stage cross-cutting vein geometries, including fold-hinge normal, sub-vertical A–C and shallowly-dipping A–B veins, indicate veining during the fold lock up stage. Fold lock up occurs during the amplification and tightening of folds, when fold limbs rotate to dips > ca. 65–70° (Fowler and Winsor, 1997; Kisters, 1995). At this stage, further tightening of the fold can no longer be accommodated through flexural slip as the limbs have rotated to high angles to the regional shortening strain. Instead, fold tightening is accomplished by internal shortening of the fold and extensional fracturing that can accommodate the local stretch at high angles to the regional shortening strain. This is the stage where the highly discordant A–C and sub-horizontal A–B veins are likely to have formed. The orientation of the vein sets suggests a component of sub-horizontal, NE-trending, fold-hinge-parallel extension (A–C veins) combined with near-orthogonal sub-vertical stretch (A–B veins) normal to NW-directed, subhorizontal shortening (D2). The bulk of the gold mineralization is hosted by these late vein sets and, similar to the Kalukwete and Mapuli prospects along the detachment, point to the introduction of the gold mineralization late in the evolution of the fluid system. This corresponds to the late-stage gold mineralization associated with cross-cutting vein sets (Hodgson, 1989; Kisters, 1995) or late-stage high-angle reverse faults (e.g. Cox et al., 2001; Schaubs and Wilson, 2002; Willman 2007) documented from many fold-and-thrust belts worldwide, where fracturing and veining accommodate the internal shortening of folds.

Mineralization in particularly the central, mafic sill emphasizes the significance of both mechanical and chemical controls for focused fluid flow and gold precipitation. The concentration of veins along the sill underlines the competence of the mafic rocks compared to the enveloping schists of the Muyaga Group during folding. The close spatial association between auriferous quartz veins and syn-D2 pyrite in wall rocks illustrates the importance of wall-rock sulphidation reactions for gold precipitation (e.g., Mikucki, 1998), particularly in and along ferruginous mafic sills.

7.3. Fluid sources

Quartz veins associated with D2 fluid flow all have relatively high $\delta^{18}O$ values from 11.6–12.9‰ in the basement, and 12.4–16.4‰ in the Upper Muyaga Group (Fig. 14). These values are typical of clastic sedimentary rocks such as slates and quartzites of the Muyaga Group (Bindeman, 2008 and references therein). The massive quartz veining at Mapuli arguably indicates the area with the highest fluid throughput. Thus, $\delta^{18}O$ values of up to ca. 16‰ for set 3 quartz veins at Mapuli are likely to be the best reflection of the original $\delta^{18}O$ composition of the fluid. Fluid sources may be related to the dehydration of pelitic rocks and/or meteoric fluids that equilibrated with the supracrustal rocks. Pre-D2 shear veins in basement gneisses have lower $\delta^{18}O$ values of

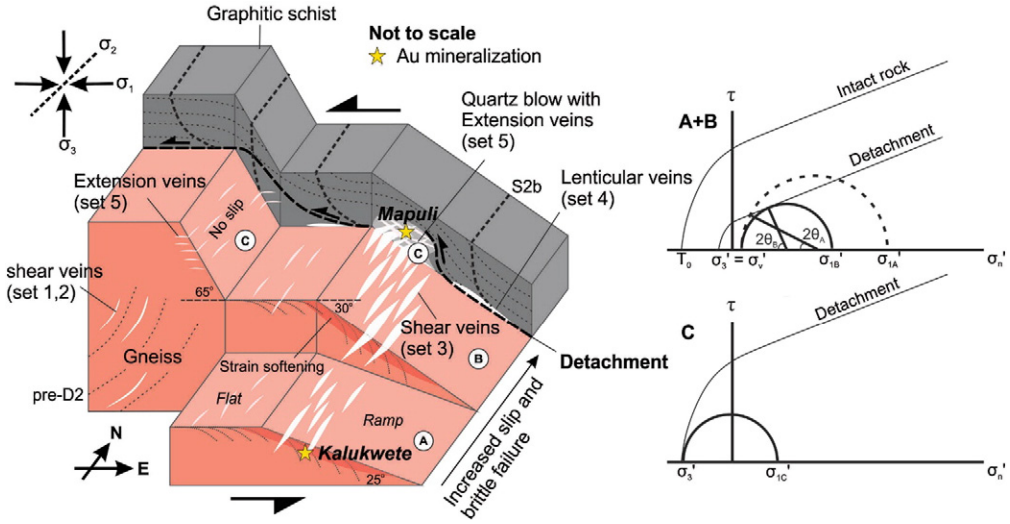

Fig. 15. Schematic diagram of ramp structures along the detachment and general quartz vein geometries and abundances. Locations A, B and C are described with Mohr-Coulomb diagrams showing conditions for failure along shallow to steep dipping sections of the detachment ($\theta_A = 25°$; $\theta_B = 30°$; $\theta_C = 65°$). The regional stress orientation is inferred to be vertical for σ1 and σ2, and parallel with the strike of the detachment. Note orientation of ramp B is most favourable for the initiation of slip (e.g. Fagereng et al., 2014).

8.2–10.1‰, which may indicate fluid of igneous or metamorphic origin unrelated to the D2 event.

Variations in $\delta^{18}O$ values for D2 quartz veins are largely attributed to wall-rock buffering either by basement gneisses, or mafic sills in the cover, which partially lower $\delta^{18}O$ values (Fig. 14). A clear example of this can be seen at Mtakuja where late A-B veins, hosted within a prominent mafic sill, have lower than expected $\delta^{18}O$ values of 12.4–12.7‰. By comparison quartz veins in adjacent slate or quartzite have $\delta^{18}O$ values above 16‰ (e.g. Mapuli). Note that the quartz vein $\delta^{18}O$ values show a strong correlation with the host $\delta^{18}O$ values ($r = 0.74$), indicating a 'rock-buffered' fluid system (e.g. Gray et al., 1991).

Considering the relationship between fluid flow and D2 deformation (e.g. Koegelenberg et al., 2015), fluids are likely to have originated from low-grade metamorphism and dehydration of the Kagera Supergroup, and specifically the metapelitic Muyaga Group This is consistent with a rock-buffered fluid system. Stable isotope data do not indicate the influx of water from external sources and input of magmatic or surface waters. This also suggests an internally generated fluid and a closed fluid system (e.g. Kenis et al., 2000; Oliver et al., 1993). If a meteoric fluid source was assumed, the fluid would have to exchange with the host rocks very thoroughly. Given the only lower-greenschist-facies grades of syn-D2 metamorphism, basement TTG gneisses, chlorite schists and amphibolites of the MN inlier are unlikely to have contributed to the mineralizing fluid. This also suggests that the source of gold is not associated with the gold endowed Archaean greenstones of the TC, but rather inclusive of rocks that constitute the KAB (e.g. Kabete et al., 2012). More local and subtle oxygen isotope variations are likely the result of fluid mixing from different metasedimentary packages and interlayered mafic sills and dykes in the Kagera Supergroup (e.g. Berwouts et al., 2008).

8. Conclusion

Exploration of traditional greenstone-hosted gold deposits on the Tanzania Craton has reached a fairly mature stage and requires the identification of deposits outside the boundaries of the Archaean granitoid-greenstone basement. In this paper, we have described the occurrence and controls of gold prospects that are mined on a regional scale along the NW margin of the craton that is structurally overlain by Mesoproterozoic low-grade metamorphic sediments of the Karagwe-Ankole fold-and-thrust belt. Regional-scale fluid flow and gold mineralization are largely confined to the sheared low-angle detachment between Archaean basement gneisses and younger, allochthonous cover rocks. The formation of auriferous quartz veins is primarily controlled by the pronounced competence contrast between weak detachment rocks and competent quartzo-feldspathic footwall gneisses that promote brittle fracturing and veining. Gold mining concentrates around subtle ramp structures within the gently undulating detachment. The gently-inclined ramps are more optimally orientated (20°–45°) for fault slip and repeated reactivation of the detachment, thus, enhancing brittle fracture permeabilities in the underlying gneisses. Gold mining in the stratigraphically higher section above the main detachment in metasediments of the Muyaga Group is closely associated with fold structures of the main fold-and-thrust belt. Quartz veins are again preferentially developed in competent units such as quartzites and dolerite sills. Overprinting vein generations record fluid infiltration during fold amplification and fold tightening. The bulk of the gold mineralization is associated with late-stage cross-cutting veins that document veining during the lock-up stage of the tight folds and orthogonal extension normal to the regional shortening strains.

Oxygen isotope data suggest that dehydration of the low-grade metapelites and minor metapsammites of the overlying Karagwe-Ankole Belt represented the likely fluid source of this regional-scale fluid system. Given the extent (>100 km) of the main detachment and the artisanal mining that can intermittently be traced along much of this basement-cover contact, makes this region overlying the western margin of the Tanzania Craton a potentially significant gold province.

Acknowledgements

This project would not have been possible without the financial and logistical support from Anglo Gold Ashanti Exploration (AGA) and the results are published with permission from AGA. A special thanks to Esperius Kavako who provided invaluable guidance in the field as an assistant, and Gillian Williams for her thorough management of the exploration project. Special thanks to Joas Kabete, and the late Pieter Winkler who initiated the project. Thanks also to Stellenbosch University's Central Analytical Facilities and Anton du Plessis for the use of their advanced nano-CT scanner. Bursary funding is also greatly appreciated from AGA, as well as an NRF Scarce Skills Development Grant (81573) to C. Koegelenberg. Gregor Borg and Phillipe Muchez are thanked for their very helpful reviews and Paul Duuring for expert editorial handling.

References

Berwouts, I., Van Roorden, M., Muchez, P.H., Boyce, A.J., Sintubin, M., 2008. Inferring intermediate-scale fluid flow in a heterogeneous metasedimentary multilayer sequence during progressive deformation: evidence from the Monts d'Arre'e slate belt (Brittany, France). Geofluids 8, 143–158.

Bindeman, I., 2008. Oxygen isotopes in mantle and crustal magmas as revealed by single crystal analysis. Rev. Mineral. Geochem. 69, 445–478.

Borg, G., Krogh, T., 1999. Isotopic age data of single zircons from the Archaean Sukumaland Greenstone Belt Tanzania. J. Afr. Earth Sci. 29, 301–312.

Borg, G., Shackleton, R.M., 1997. The Tanzania and NE-Zaire cratons. In: De Wit, M., Ashwal, L.D. (Eds.), Greenstone Belts. Oxford University Press, pp. 608–619.

Cahen, L., Snelling, N.J., Delhal, J., Vail, J.R., Bonhomme, M., Ledent, D., 1984. The geochronology and evolution of africa. Oxford University Press, Oxford 512 pp.

Coggon, R., Holland, T.J.B., 2002. Mixing properties of phengitic micas and revised garnet-phengite thermobarometers. J. Metamorph. Geol. 20 (7), 683–696.

Cox, S.F., Knackstedt, M.A., Braun, J., 2001. Principles of structural control on permeability and fluid flow in hydrothermal systems. Rev. Econ. Geol. 14, 1–24.

De Waele, B., Johnson, S.P., Pisarevski, S.A., 2008. Palaeoproterozoic to Neoproterozoic growth and evolution of the eastern Congo Craton: its role in the Rodinia puzzle. Precambrian Res. 160, 127–141.

Deblond, A., Punzalan, L.E., Boven, A., Tack, L., 2001. The Malagarazi Supergroup of SE Burundi and its correlative Bukoban Supergroup of NW Tanzania: Neo- and Mesoproterozoic chronostratigraphic constraints from Ar–Ar ages on mafic intrusive rocks. J. Afr. Earth Sci. 32, 435–449.

Duuring, P., Hagemann, S., Love, R.J., 2001. A thrust ramp model for gold mineralization at the Archean Trondhjemite-hosted Tarmoola deposit: the importance of heterogeneous stress distributions around granitoid contacts. Econ. Geol. 96, 1379–1396.

Eiler, J., Stolper, E.M., McCanta, M.C., 2011. Intra- and intercrystalline oxygen isotope variations in minerals from basalts and peridotites. J. Petrol. 52 (7–9), 1393–1413.

Evans, D.M., Boadi, I., Byemelwa, L., Gilligan, J., Kabete, J., Marcet, P., 2000. Kabanga magmatic sulphide deposits, Tanzania: morphology and geochemistry of associated intrusions. J. Afr. Earth Sci. 30, 651–674.

Fagereng, Å., Smith, Z., Rowe, C.D., Makhubu, B., Sylvester, F.Y.G., 2014. Stress, strain, and fault behavior at a thrust ramp: insights from the Naukluft thrust, Namibia. J. Struct. Geol. 58, 95–107.

Fernandez-Alonso, M., Cutten, H., De Waele, B., Tack, L., Tahon, A., Baudet, D., Barritt, S.D., 2012. The Mesoproterozoic Karagwe-Ankole Belt (formerly the NE Kibara Belt): the result of prolonged extensional intracratonic basin development punctuated by two short-lived far field compressional events. Precambrian Res. 216-219, 63–86.

Fowler, T.J., Winsor, C.N., 1997. Characteristics and occurrence of bedding-parallel slip surfaces and laminated veins in chevron folds from the Bendigo-Castleman goldfields: implications for flexural-slip folding. J. Struct. Geol. 19, 799–815.

Fritz, H., Abdelsalam, M., Ali, K.A., Bingen, B., Collins, A.S., Fowler, A.R., Ghebreab, W., Hauzenberger, C.A., Johnson, P.R., Kusky, T.M., Macey, P., Muhongo, S., Stern, R.J., 2013. Orogen styles in the East African Orogen: a review of the Neoproterozoic to Cambrian tectonic evolution. J. Afr. Earth Sci. 86, 65–106.

Gray, D.R., Gregory, R.T., Durney, D.W., 1991. Rock-buffered fluid-rock interaction in deformed quartz-rich turbidite sequences, eastern Australia. Journal of Geophysical Research 96, 19 681–19 704.

Harris, C., Ashwal, L.D., 2002. The origin of low d18O granites and related rocks from the Seychells. Contrib. Mineral. Petrol. 143 (3), 366–376.

Harris, C., Vogeli, J., 2010. Oxygen isotope composition of garnet in the Peninsula Granite, Cape Granite Suite, South Africa: constraints on melting and emplacement mechanisms. S. Afr. J. Geol. 113 (4), 385–396.

Hodgson, C.J., 1989. The structure of shear-related, vein-type gold deposits: a review. Ore Geol. Rev. 4, 231–273.

Kabete, J.M., Groves, D.I., McNaughton, N.J., Mruma, A.H., 2012. A new tectonic and temporal framework for the Tanzanian Shield: implications for gold metallogeny and undiscovered endowment. Ore Geol. Rev. 48, 88–124.

Kenis, I., Muchez, Ph., Sintubin, M., Mansy, J.L., Lacquement, F., 2000. The use of a combined structural, stable isotopic and fluid inclusion study to constrain the kinematic history at the northern Variscan front zone (Bettrechies, France). J. Struct. Geol. 22, 598–602.

Kisters, F.M., 1995. Controls of gold-quartz vein formation during regional folding in amphibolite-facies, marble-dominated meta-sediments of the Navachab Gold Mine in the Pan-African Damara Belt, Namibia. S. Afr. J. Geol. 108, 365–380.

Koegelenberg, C., Kisters, A.F.M., 2014. Tectonic wedging, back-thrusting and basin development in the frontal parts of the Mesoproterozoic Karagwe-Ankole belt in NW Tanzania. J. Afr. Earth Sci. 97, 87–98.

Koegelenberg, C., Kisters, A.F.M., Kramers, J.D., Frei, D., 2015. U–Pb detrital zircon and ^{39}Ar–^{40}Ar muscovite ages from the eastern parts of the Karagwe-Ankole Belt: tracking Paleoproterozoic basin formation and Mesoproterozoic crustal amalgamation along the western margin of the Tanzania Craton. Precambrian Res. 269, 147–161.

Mäkitie, H., Data, G., Isabirye, E., Manttari, I., Huhma, H., Klausen, M.B., Pakkanen, L., Virransalo, P., 2014. Petrology, geochronology and emplacement model of the giant 1.37 Ga arcuate Lake Victoria Dyke Swarm on the margin of a large igneous province in eastern Africa. J. Afr. Earth Sci. 97, 273–297 c.

Mikucki, E.J., 1998. Hydrothermal transport and depositional processes in Archean lode-gold systems: a review. Ore Geol. Rev. 13, 307–321.

Nguyen, P.T., Cox, S.F., Harris, L.B., Powell, C.M., 1998. Fault-valve behaviour in optimally orientated shear zones: an example at the Revenge gold mine, Kambalda, Western Australia. J. Struct. Geol. 20, 1625–1640.

Ojala, V.J., Ridley, J.R., Groves, D.I., Hall, G.C., 1993. The Granny Smith gold deposit: the role of heterogeneous stress distribution at an irregular granitoid contact in a greenschist-facies terrane. Mineral. Deposita 28, 409–419.

Oliver, N.H.S., Cartwright, I., Wall, V.J., Golding, S.D., 1993. The stable isotope signature of kilometre-scale fracture dominated metamorphic fluid pathways, Mary Kathleen, Australia. J. Metamorph. Geol. 11, 705–720.

Oliver, N.H.S., Ord, A., Valenta, R.K., Upton, P., 2001. Deformation, fluid flow, and ore genesis in the in the heterogeneous rocks, with examples and numerical models from the Mount Isa district, Australia. Rev. Econ. Geol. 14, 51–74.

Powell, R., Evans, J.A., 1983. A new geobarometer for the assemblage biotite-muscovite-chlorite-quartz. J. Metamorph. Geol. 1 (4), 331–336.

Schaubs, P.M., Wilson, C.J.L., 2002. The relative roles of folding and faulting in controlling gold mineralization along the Deborah Anticline, Bendigo, Victoria, Australia. Econ. Geol. 97, 351–370.

Seward, T.M., 1973. The complexes of gold and the transport of gold in hydrothermal gold solutions. Geochim. Cosmochim. Acta 37, 379–399.

Sibson, R.H., Scott, J., 1998. Stress/fault controls on the containment and release of overpressured fluids: examples from gold-quartz vein systems in Juneau, Alaska; Victoria, Australia and Otago, New Zealand. Ore Geol. Rev. 13, 293–306.

Sibson, R.H., Robert, F., Poulsen, K.H., 1988. High-angle reverse faults, fluid-pressure cycling, and mesothermal gold-quartz deposits. Geology Vol. 16, 551–555 (Groves et al., 1998; 2000).

Tack, L., Liégeois, J.P., Deblond, A., Duchesne, J.C., 1994. Kibaran A-type granitoids and mafic rocks generated by two mantle sources in a late orogenic setting (Burundi). Precambrian Res. 68, 323–356.

Tack, L., Wingate, M.T.D., De Waele, B., Meert, J., Belousova, E., Griffin, A., Tahon, A., Fernandez-Alonso, M., 2010. The 1375 Ma "Kibaran event" in Central Africa: prominent emplacement of bimodal magmatism under extensional regime. Precambrian Res. 180 (2010), 63–84.

Tanzania Chamber of Mines and Energy, 2015. (Website) http://www.tcme.or.tz/mining-in-tanzania/industry-overview/.

Willman, C.E., 2007. Regional structural controls of gold mineralisation. Bendigo and Castlemaine goldfields, Central Victoria, Australia 42 (5), 449–463.

Westerhof, A.B.P., Härmä, P., Isabirye, E., Katto, E., Koistinen, T., Kuosmanen, E., Letho, T., Lehtonen, M.I., Mäkitie, H., Manninen, T., Mänttäri, I., Pekkala, Y., Pokki, J., Saalmann, K., Virransalo, P., 2014. Geology and geodynamic development of Uganda with explanation of the 1:1,000,000 scale geological map. Geological Survey of Finland, Special Paper 55.

Zhu, Y., An, F., Tan, J., 2011. Geochemistry of hydrothermal gold deposits: a review. Geosci. Front. 2 (3), 367–374.